Winter 12-15-2018

KCNQ1/KCNE1 Interaction in the Cardiac IKs Channel and its Physiological Consequences

Jiajing Xu
Washington University in St. Louis

WASHINGTON UNIVERSITY IN ST. LOUIS
Department of Biomedical Engineering

Dissertation Examination Committee:
Yoram Rudy, Chair
Jianmin Cui
Vitaly Klyachko
Richard Schuessler
George Van Hare

KCNQ1/KCNE1 Interaction in the Cardiac IKs Channel and its Physiological Consequences

By
Jiajing Xu

A dissertation presented to
The Graduate School
of Washington University in
partial fulfillment of the
requirements for the degree
of Doctor of Philosophy

December 2018
St. Louis, Missouri

Table of Contents

List of Figures

List of Tables

Acknowledgments

First gratitude to my parents for all the way you lead me from nowhere, all the heart-to-heart talks whether I have been able to express myself and all the understanding of my choices. I once thought I had spent all my luck to be born with such two lifelong friends, who would never leave.

Special thanks to Dr. Rudy for all the supports for this dissertation, all the guides through the academic difficulties and all the discussions that helped me out of doubts in life.

Last but not least, I would like to appreciate the people I have met in Rudy Lab, in Washington University in St. Louis and on my way travelling across the United States. With all of you here, I enjoyed St. Louis, a city so different from where I was born. With all of you with me, I praised all the mountains, lakes, forests and sand dunes. Whether photographed or not, I would like to carry all the memories with me.

So long, and thanks for all the sunsets.

Jiajing Xu

Washington University in St. Louis

December 2018

“Don’t Panic!”

— Douglas Adams, The Hitchhiker's Guide to the Galaxy

ABSTRACT OF THE DISSERTATION

KCNQ1/KCNE1 Interaction in the Cardiac IKs Channel and its Physiological Consequences

by

Jiajing Xu

Doctor of Philosophy in Biomedical Engineering

Washington University in St. Louis, 2018

Professor Yoram Rudy, Chair

Dynamic conformational changes of ion channel proteins during activation gating determine their function as carriers of current. The relationship between these molecular movements and channel function over the physiological timescale of the action potential (AP) has not been fully established due to limitations of existing techniques. We constructed a library of possible cardiac IKs protein conformations and applied a combination of protein segmentation and energy linearization to study this relationship computationally. Simulations reproduced the effects of the beta-subunit (KCNE1) on the alpha-subunit (KCNQ1) dynamics and function, observed in experiments. Mechanistically, KCNE1 increased the probability of "visiting" conducting pore conformations on activation trajectories, thereby increasing IKs current. KCNE1 slowed IKs activation by impeding the voltage sensor (VS) movement and reducing its coupling to pore opening. Conformational changes along activation trajectories determined that the S4-S5 linker (S4S5L) plays an important role in these modulatory effects by KCNE1. Integration of these molecular structure-based IKs dynamics into a model of human cardiac ventricular myocyte, revealed that KCNQ1-KCNE1 interaction is essential for normal AP repolarization.

Chapter 1 Introduction

1.1. History of IKs Channel Discovery

Electrical activity plays an essential role in the functioning of cardiac cells; the cyclic changes of membrane potential of myocytes underlie their repetitive and periodic excitation and contraction. This voltage cycle, so called action potential (AP), could be roughly divided into depolarization (the 'upstroke'), plateau, repolarization and resting phases (denoted as phase 1 to 4, respectively). Each phase is supported and controlled by a network of various ion channels, pumps and other membrane transport proteins. During the repolarization process, the membrane potential of a myocyte drops from positive values back to its resting negative value and finally terminates the cardiac AP. When the ventricular myocardium starts to repolarize and how fast it repolarizes, that is, the shape and duration of phase 2 and 3 of its AP, is reflected in the QT interval on the electrocardiogram (ECG). Repolarization during phase 3 is mainly determined by three potassium currents, which constitute the "repolarization capacity" – the fast and slow delayed rectifier currents, IKr and IKs (shown in Figure 1.1), and the time-independent potassium current, IK1 [Luo 1994]. Defects in these currents lead to cardiac

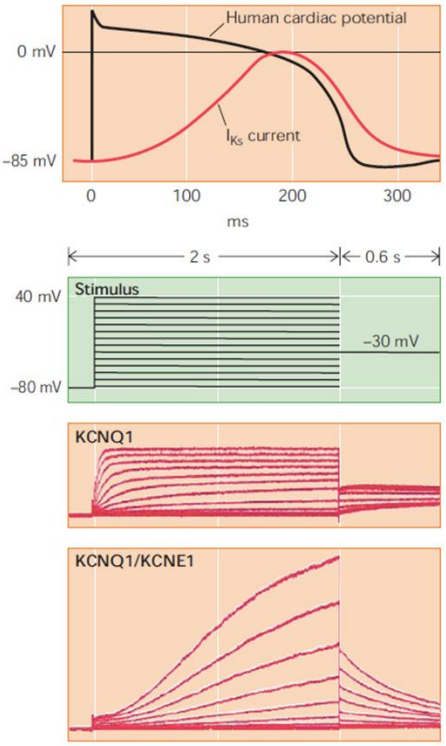

Figure 1.1, top: Action potential and IKs during the AP; bottom: Macroscopic currents of KCNQ1 with or without KCNE1 co-expressed [Jespersen 2005].

arrhythmias presenting a prolonged QT interval in patients' ECG signal (Long QT or LQT syndrome). Among them, IKs is the main current that increases at fast heart rates to shorten the AP duration (APD), and is subject to β-adrenergic regulation [Terrenoire 2005]. IKs is also important for AP restitution during premature beats [O'Hara 2011].

In 1996, a potassium pore-forming protein was found to be the major component (α-subunit) of the ion channel carrying the IKs current and to be responsible for the human LQT syndrome type1 (LQT1) [Wang 1999, Yang 1997]. Thus, this protein was initially called KvLQT1, but later named KCNQ1 or Kv7.1 based on the Gene Nomenclature (http://www.genenames.org/). The primary translated KCNQ1 subunit consists of 676 residues forming six transmembrane domains and a pore loop with a typical potassium-channel pore-signature sequence (TIGYG), as shown in Figure 1.2. Four KCNQ1 proteins assemble to form a functional channel. As a voltage-dependent ion channel, the voltage sensor of KCNQ1 is located at the S4 segment. The S4-S5 linker (S4S5L) also affects activation gating, while the inactivation process is carried by the S5 helix and the pore loop. Inactivation is a C-terminus dependent process, known as C-type inactivation. When the membrane undergoes depolarization, the voltage-gated KCNQ1 channel produces a relatively fast activating and deactivating potassium current compared to the IKs current, under the same voltage protocol [Jespersen 2005].

Later, the KCNQ1 subunits were found to be tightly regulated by auxiliary proteins (β-subunits, KCNE1) and other accessory factors in the human heart. Co-expression of KCNQ1 with KCNE1 subunits is required to generate the IKs current in cardiac cells. KCNE1, composed of 129 residues, is a relatively small protein containing only one transmembrane segment (Figure 1.2). In its presence, the macroscopic potassium flux through the KCNQ1/KCNE1 complex (that is, the IKs channel) shows a significant increase in its amplitude, slower activation and deactivation

processes, a removal of inactivation, and a positive shift in the voltage dependence of channel activation (shown in Figure 1.1) [Barhanin 1996, Sanguinetti 1996]. Mutations in the KCNE1 subunits can also cause defects in IKs channel function, leading to type-5 LQT syndrome (LQT5, corresponding to LQT1 caused by KCNQ1 mutations).

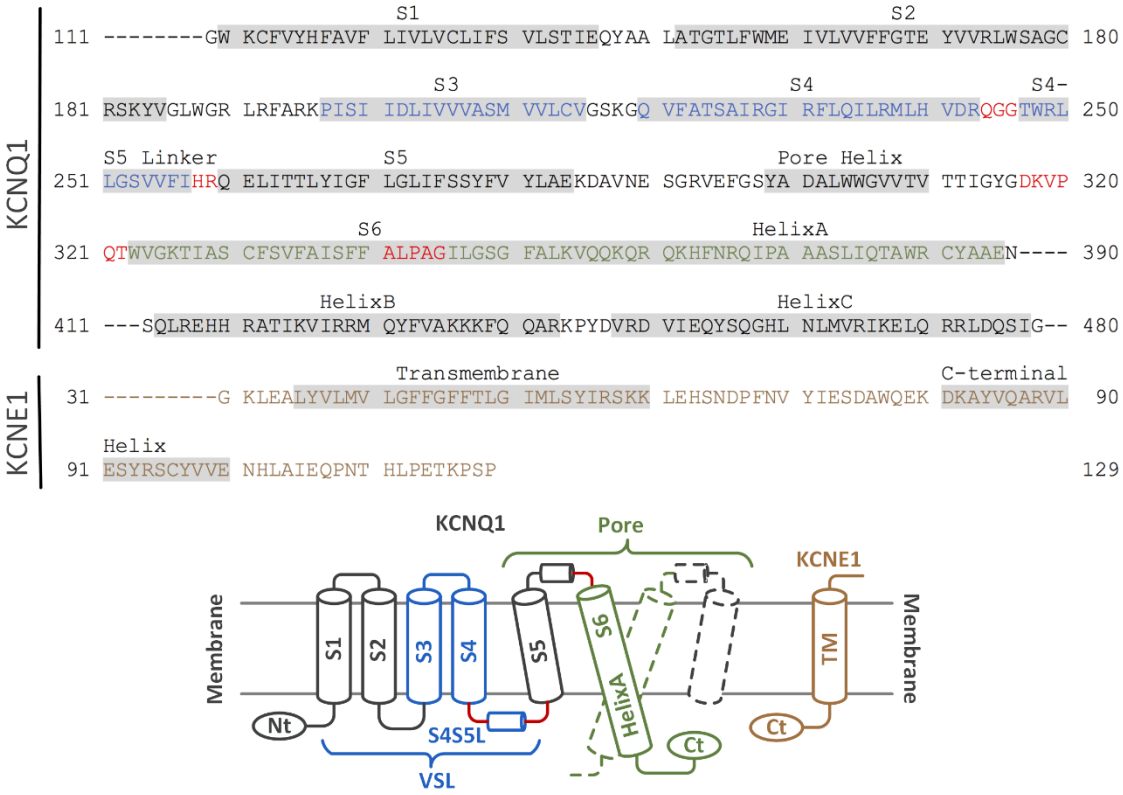

Figure 1.2, Sequence of KCNQ1 (top) and KCNE1 (bottom) residues included in the construction of KCNQ1 and IKs structures in this simulation study. Other residues of the protein have been omitted and marked in the figure by a dashed line. Alpha helices are shaded. Residues with dihedral angles that were varied to construct the structural library are listed in red. The protein segments that comprise these structural components are shown in the color-coded cartoon on the bottom; VSL: S1-S4 and S4S5L, Pore: S5-S6 and the proximal C-terminus.

1.2. Recent findings of IKs channel Studies

The pore-forming subunit (KCNQ1) is homologous to Kv1.2, for which a crystal structure has been resolved [Long 2007]. The structure of the accessory subunit (KCNE1) has been determined

using nuclear magnetic resonance spectroscopy (NMR) [Kang 2008]. These determined structures provided a starting template for constructing the structure of the transmembrane domain of IKs in this study. A molecular model of the KCNQ1/KCNE1 channel complex was constructed by Kang and his co-workers using Rosetta-Dock program in 2008. By docking the KCNE1 transmembrane segment in the space between the pore domain and the voltage sensing domains from adjacent KCNQ1 subunits, they provided an approximation of the KCNE1 docking site in the KCNQ1 channel. Their research also sketched the conformational change of the channel complex between the open and closed states. A crystal structure of S6-Helix A-Helix B clamped with calmodulin (CaM) [Sachyani 2014] and a recently published cryo-EM structure of the KCNQ1/CaM complex [Sun 2017] provided additional structural information on the cytosolic domain of IKs.

Like other voltage-gated potassium channels [Papazian 1995], the positively charged S4 segment of KCNQ1 moves up (toward the extracellular space) across the membrane in response to depolarization. Experimental studies suggested that S4S5L also plays an important role in IKs gating [Choveau 2011, Labro 2011, Lvov 2010, Sun 2017]. Experiments have shown that KCNE1 slows the activation of IKs and increases its macroscopic current but there is no consensus about the structure-based mechanisms of these effects. These studies concluded that KCNE1 slows KCNQ1 activation either by slowing the S4 movement [Ruscic 2013] or by suppressing the coupling between the voltage sensor (VS) movement and pore opening [Osteen 2010, Barro-Soria 2014].

Recent experiments lead to two other debates about the IKs channel: (1) Is the gating of IKs cooperative or sequential [Meisel 2012]? How is it different with and without KCNE1? (2) Under physiological conditions, is the KCNQ1:KCNE1stoichiometry of IKs fixed at 4:2 [Plant 2014] or

variable between 4:1 to 4:4 [Murray 2016, Nakajo 2010]? What is the effect of different stoichiometries on IKs activation and the AP?

1.3. From Structure to Function

Crystallography, NMR and other imaging techniques provided detailed information on ion channels molecular structure. However, the information is limited to protein conformations 'frozen' at particular membrane conditions and therefore difficult to relate to kinetic functional data from fluorescence, voltage clamp and other experimental recordings. Molecular dynamics (MD) simulations have provided insights on possible conformational changes of proteins at pico-seconds resolution. However, it required extreme non-physiological membrane voltages and weeks of computing time for a customized super-computer to simulate a single trajectory of conformational changes during 250 micro-seconds gating of a Kv1.2-Kv2.1 chimera [Jensen 2012]. Clearly, simulation of ion-channel gating at the atomistic scale, over the physiological time course of the AP (milliseconds for nerve and muscle; hundreds of milliseconds for the cardiac AP) is impossible with direct computing and commonly used MD methods.

Here, we present a framework for computing conformational changes of an ion channel protein over the time scale of activation gating and determine mechanistic relationships between conformational changes and electrophysiological function. While it builds on our previous work [Nekouzadeh 2008, Nekouzadeh 2011, Nekouzadeh 2016, Silva 2009], it advances it in the following major ways that are important for elucidating mechanisms: (1) Simulations are conducted on an atomistic scale, at a resolution of <1.0Å and with all molecular details included. (2) Tetrameric symmetry of the protein is not assumed. (3) Concerted movement between the four VS and cooperativity in activation gating are also not assumed. (4) A much higher number of degrees of freedom for molecular movement are considered in the computations. (5) KCNE1 is

docked into the KCNQ1 structure and included explicitly in the simulations. This is accomplished by generating a large library of possible protein structures, which covers the conformational space that the ion channel can occupy during gating, and by dissecting the protein into structural segments and linearizing calculations of protein energy. We used the computational approach to study mechanisms of KCNQ1-KCNE1 interactions and their effects on IKs activation and the human cardiac ventricular AP. We determined the role of specific segments and residues of KCNQ1 and KCNE1 during channel gating and identified key residues that influence the activation kinetics, with emphasis on the S4S5L that couples the voltage sensor domain of the channel to its pore. The computational approach allowed us to integrate across scales, from the molecular structure of IKs to the whole-cell AP.

Chapter 2 Materials and Methods

Achieving the objectives of this study required simulation of KCNQ1 and IKs activation based on their detailed molecular structures at atomistic scale. Direct computing of the gating movement over the relevant time scale (tens of milliseconds) is not possible. To overcome this difficulty, the strategy depicted in Figure 2.1 was employed. KCNQ1 and IKs structural libraries were constructed and constrained based on biophysical considerations and experimental data. The libraries contained more than 10^{30} conformations and covered the conformational space of possible structures during activation gating. The electrostatic energy of each possible conformation was computed using the Generalized Born Equation. For the energy computation, the protein was divided virtually into structural elements, based on functional role during activation. These included VSL - the VS domain coupled to the S4-S5 linker (S4S5L), the pore domain and KCNE1 (Figures 1.2 and 2.1). Energy was computed for each element and through superposition for the entire protein. This approach was motivated by the need to circumvent the (impossible) intense computing requirement for direct computation of the entire protein energy for all possible conformations. It also allowed us to determine the energy contributions from different elements of the protein and their interactions. To simulate the dynamics of KCNQ1 and IKs during activation, trajectories were generated in conformation space based on the energy landscape. General methodology procedures are described below.

2.1. Definitions and Properties

Coordinate system and discretization: A Cartesian coordinate system (Figure 2.1B in the main text) was defined in the lipid-water system. The KCNQ1 and KCNE1 templates were aligned with these coordinates. The x-y plane slices through the middle of the lipid membrane; the z-axis passes

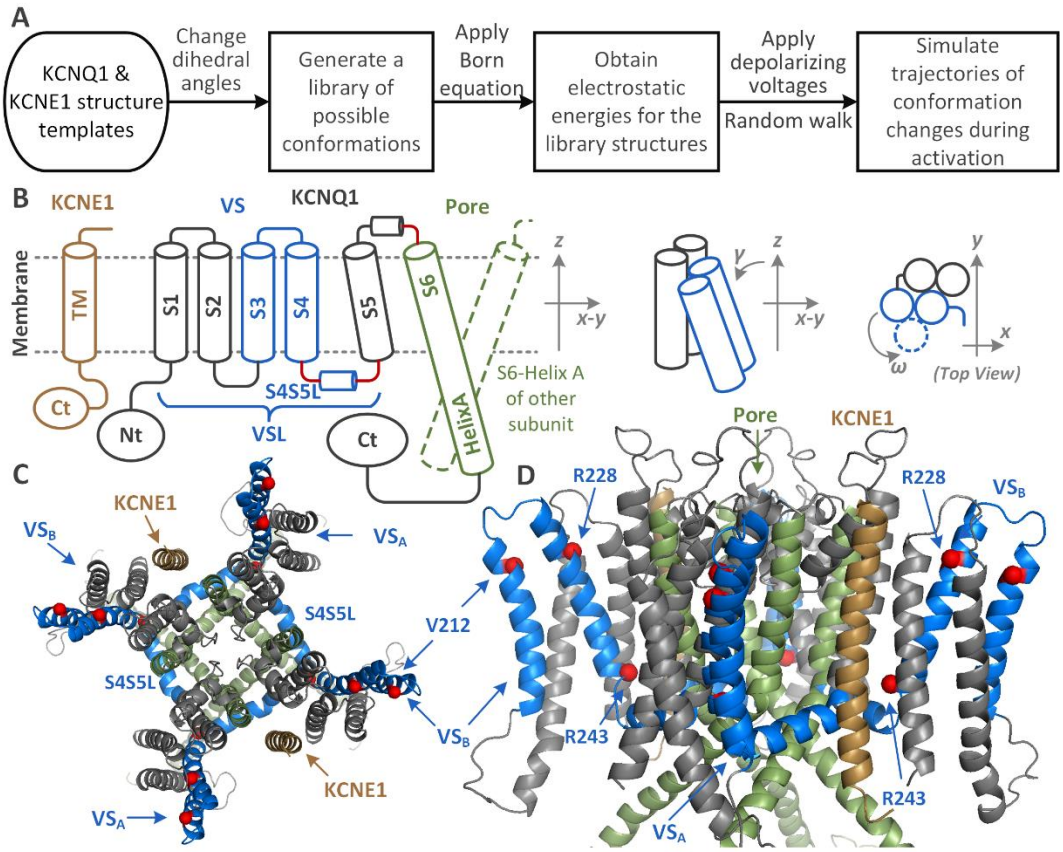

Figure 2.1, (A) Flowchart for simulating channel activation. (B) Diagrams defining structural elements of IKs and coordinate system. Linkers with dihedral angles that were varied during construction of the structural library are colored red. (C) Top view of a representative conformation from the IKs library. Cytosolic domain of the channel is omitted here; a complete representative KCNQ1 structure is shown in Figure 2.2. Two KCNE1 subunits (brown) are inserted in opposite pockets of the KCNQ1 protein. Two types of voltage sensors (VS_A and VS_B) are distinguished, based on their proximity and interactions with KCNE1; S3 and S4 (blue) of VS_A face KNCE1, S1 and S2 (gray) of VS_B face KCNE1. (D) Side view of the same conformation. The alpha carbons of V212, R228 and R243 are shown as red spheres. VS, voltage sensor; S4S5L, S4-S5 linker; VSL, VS and S4S5L combined; TM, transmembrane segment; Nt, N-terminus; Ct, C-terminus. Color code (for Figures 2.1 and 2.2) is defined in the diagram of panel B.

through the center of the KCNQ1 selectivity filter with its positive direction pointing towards the extracellular space. To estimate the volume occupied by KCNQ1 and assign non-uniform

dielectric properties to the protein-lipid-water system, the space was discretized into cubical elements of dimensions 0.5Å x 0.5Å x 0.5Å.

Resolution of the structural libraries: Dihedral angles of protein residues were sampled at a 4° resolution. The conformational space is discretized uniformly in dihedral angles, but not in translation and rotation in the Cartesian coordinate system. Root-mean-square-deviation (RMSD) was used to estimate the Cartesian grid size of the library. For every conformation in the library,

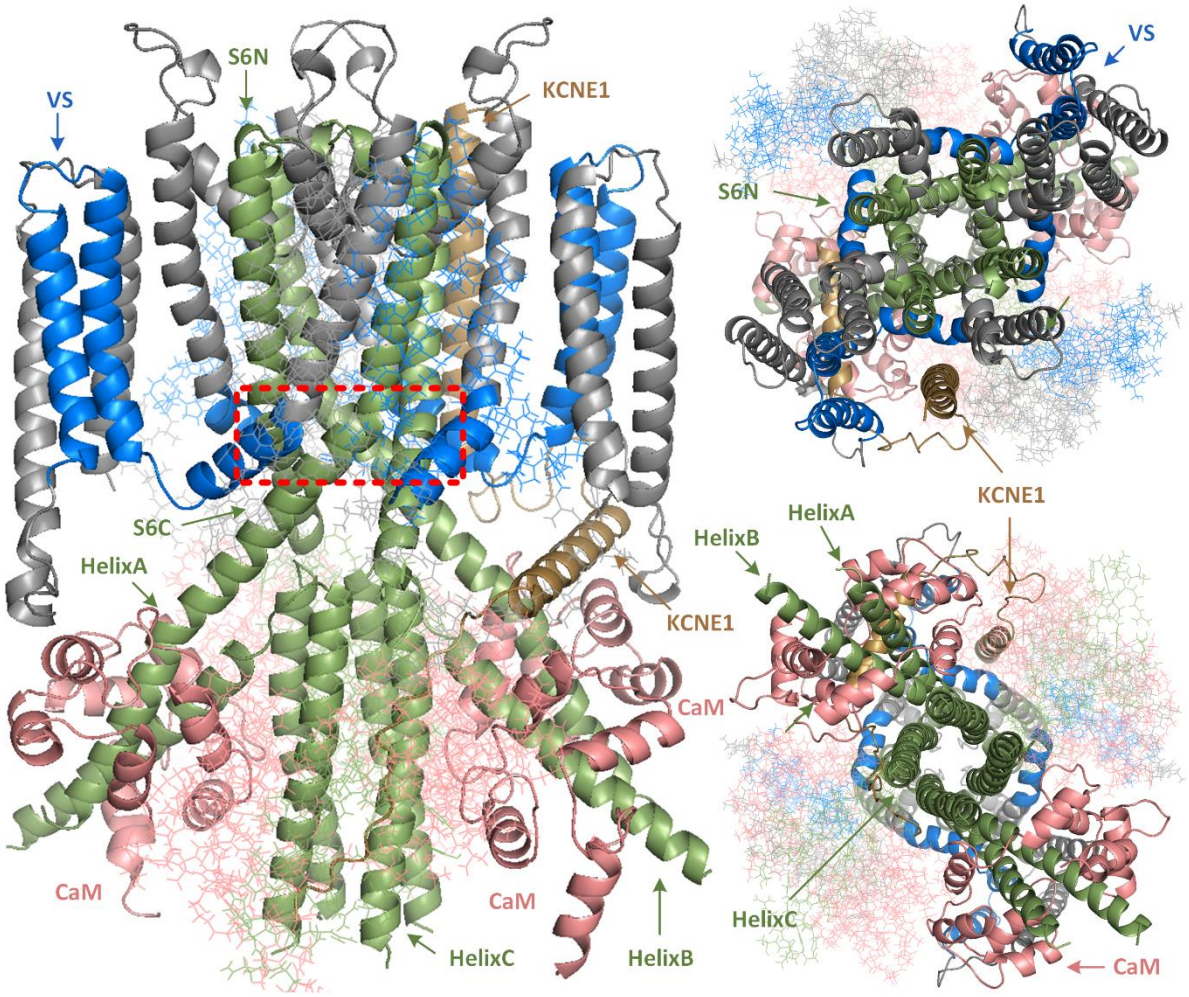

Figure 2.2. Detailed visualization of the IKs structure shown in Figure 2.1 (the structure shown in Figure 2.1 is simplified). This is one structure in the library. Left: side view; Right, top: top view; Right, bottom: bottom view. Only one docked KCNE1 is shown. The PAG bend on S6 is indicated by a red box in the side view. Parts of the structure are displayed as thin lines to reveal the center of the protein. Abbreviations and color codes are the same as in Figure 2.1.

the smallest RMSD to all other conformations was between 0.3Å and 0.5Å, identifying a grid size (resolution) in this range.

Background atoms: The backbone atoms of S1, S2, S5, the pore helix and selectivity filter were defined as background atoms, assuming that they do not experience significant conformational changes during channel activation. These elements were considered static when constructing the possible S3-S4, S4S5L and S6 conformations.

Steric clashes: A conformation was considered to have steric clashes if it contained a non-bonded pair of atoms with an inter-atom distance smaller than their average van der Waals radii. Such conformations were excluded from the library.

Possible dihedral angle combinations: To generate the different conformations in the library, the dihedral angles of the following residue segments were varied: 244-246, 258-259, 317-322 and 341-345 (Figure 1.2). A combination of dihedral angles in a segment was considered possible if no steric clashes occurred between the backbone atoms and C_β atoms of the segment.

2.2. Generation of an initial structure for construction of the KCNQ1 and IKs structural libraries

An initial structure of the KCNQ1 transmembrane domain was constructed as a homology model to the crystal structure of the Kv1.2-Kv2.1 chimera (PDB: 2R9R) [Long 2007] except for the S6 segment, which was based on the crystal structure of KcsA (PDB: 3EFF). The S6 of Kv1.2 contains a PVP motif, which is absent in both KcsA and KCNQ1. S6 was extended with Helix A, which together with Helix B were clamped by calmodulin (PDB: 4V0C) [Sachyani 2014]. The distal C-terminus beyond Helix B and the N-terminus of KCNQ1 were not included, as there is no evidence for direct interactions between these segments and the VSL or the gating region of the pore domain. The transmembrane segment of KCNE1, with the residues extending its two termini,

was constructed from the NMR-determined structure (PDB: 2K21) [Kang 2008]. The initial structures for KCNQ1 and KCNE1 were inserted into a lipid membrane surrounded by water and then refined by molecular dynamics (MD) simulations. The relevant software packages are listed in Table 2.1.

The KCNQ1 initial structure was aligned with a coordinate system referenced to the membrane (Figure 2.1B). Structural elements were determined by the secondary structure of the protein. Skeletons (backbone atoms) of secondary-structure segments (Figure 1.2) were assumed to be rigid. Dihedral angles of KCNQ1 residues 258-259 (red in Figure 1.2 and red for all residues mentioned below) were varied to yield structures with different conformations of S4S5L relative to the N-terminus of S5. S4 structures with different translations and rotations were generated for each S4S5L structure by varying dihedral angles of residues 244-246. S3 was connected to S4 with a short 4-residue linker and had a very limited movement relative to S4 (<1.0Å). The pore conformation library was constructed by first computing S6 structures with different dihedral angles of KCNQ1 residues 317-322 and 341-345 and then aligning the proximal C-terminal segments to each S6. The final KCNQ1 library was determined after removal of structures with steric clashes (details in Supplement). To generate an IKs structural library, two transmembrane segments of KCNE1 were docked into the KCNQ1 protein in spaces suggested by the experiments; their position was then refined by side-chain packing for each KCNQ1 conformation. Note that the complete protein library was constructed as a combination of VSL and pore libraries. The four VSL and S6 segments of the pore were not assumed symmetric. One structure from the library is shown as an example; Figure 2.1 shows the transmembrane domain only and Figure 2.2 includes the proximal cytosolic domain. Detailed procedures are provided in the sections below.

Table 2.1. Software used in the process of constructing the structural templates for KCNQ1 and KCNE1

Tool	Application	Version	Website
Clustal W/X	Sequence comparison between KCNQ1 and Kv1.2, Kv2.1, KcsA	2.1	www.clustal.org
Modeller	Construction of KCNQ1 homology model from crystal structures	9.13	salilab.org/modeller/
PyMol	Visualization of constructed conformations; Alignment and connection of S6 and HelixA of KCNQ1	1.3 (edu)	www.pymol.org
NAMD	Refinement and equilibration of constructed structures of KCNQ1 and KCNE1	2.9	www.ks.uiuc.edu/Research/namd/

.

2.3. KCNQ1 Structural Library

2.3.1. Pore Library

The S6-HelixA complex was structured as a long alpha helix from Trp323 to Glu385 (Figures 1.2 and 2.2). A bend was located at Pro343-Ala344-Gly345 (PAG) as these residues were aligned to the PVP bending site in the homologous Kv1.2 structure [Smith 2007]. Conformations of the N-terminal section of S6 (S6N, residues 323-342) were generated by varying dihedral angles of residues 317-322, starting from the fixed end of the selectivity filter at Gly316. The constraints listed below were applied to exclude impossible conformations from the pore library:

(a) Steric clashes between atoms in residues 317-322 cannot occur.

(b) S6N should be located within the pore region, bounded by the four S5 helices; its C-terminal end should point towards the cytosolic space.

(c) There should be no steric clashes between S6N and the background atoms.

Each possible S6N conformation was extended with the C-terminal section of S6 (S6C) through PAG. The dihedral angles of PAG were varied over a range for which the secondary structure of S6 remained a continuous alpha helix, but with different degrees of bending and different orientations of its C-terminal end. Each conformation in the pore library was a tetramer, formed by four S6 segments (S6N-PAG-S6C) with the HelixA-HelixB-Calmodulin (HelixA-HelixB-CaM) motif aligned to each S6 based on the KCNQ1 template. The four S6 segments of the pore were not assumed symmetric. Criteria for determining the possibility of a pore conformation were as follows:

(d) The following steric clashes cannot occur:

I. Between atoms in PAG and Ala341-Leu342 preceding Pro343.

II. Between the backbone atoms in S6-HelixA-HelixB-CaM from different subunits.

III. Between the backbone atoms in S6-HelixA-HelixB-CaM and the background atoms.

(e) All four CaM must be in the cytosolic space (z of every atom < -20.0 Å).

(f) It must be possible to connect the distal C-terminal segment of KCNQ1, HelixC, to the end of HelixB with a five-residue linker without steric clashes between CaM and Helix C; four Helix C segments form a coiled-coil in the cytosolic space beneath the HelixA-HelixB tetramer.

(g) The side-chains of S1, S2, S5, S6 and HelixA-HelixB should be well packed within the tetramer structure.

(h) A conformation can be reached from the starting conformation through small (<1.0Å) conformational changes.

The flexibility of the 6-residue linker preceding S6N leads to a number of S6N conformations with RMSD smaller than 0.5Å between conformations. Assuming that S6N only serves to stabilize the pore structure and plays a less important role than S6C in gating, any group of conformations with S6N within 1.0Å RMSD and S6C within 0.5Å RMSD were merged into a single conformation.

The final pore library contained 615,946 conformations with a grid size of 0.5Å~1.0Å. The pore diameter of each conformation (D_{pore}) was estimated as the smallest distance between the same atoms in S6 from opposite subunits. Assuming that a pore with a larger diameter is associated with greater probability of conducting ions, the probability for a conformation to be in a conducting state, Pc, was computed as

$$Pc = \frac{1}{2}\left(\frac{2}{\sqrt{\pi}}\int_{0}^{2(D_{pore}-D_K)} e^{-x^2}dx + 1\right) \qquad (2.1)$$

where D_K is the size of a hydrated potassium ion (~6.6 Å). The probability is 0 when D_{pore} < 5.0 Å and the conformation is always conducting when D_{pore} > 8.0 Å.

2.3.2. Voltage Sensor and S4-S5 Linker (VSL) Library

We define the VSL element in the KCNQ1 library to include S3-S4 of the VS domain and the S4S5L. The S4S5L conformation space was sampled by varying the dihedral angles of His258-Arg259 (HR) preceding the fixed N-terminal end of S5. The S4 conformations were then generated by varying the dihedral angles of Gln244-Gly245-Gly246 (QGG) connected to each S4S5L (Figure 2.3). Movement of the S3 helix relative to S4 was limited by the short linker connecting them; this movement was permitted in order to prevent steric clashes, but was restricted to 1.0Å RMSD. Unlike the S6 segments from different subunits, which make direct contact, the VSL

segments of different subunits are separated by the background atoms in S1, S2 and S5. The following criteria were used to examine whether conformations of VSL are acceptable:

(a) Steric clashes between atoms in QGG and HR cannot occur (Figure 2.3).

(b) The N-terminal end of S4 should be higher than its C-terminal end in the z direction and the tilting angle of S4 from the z-axis should be smaller than 60° (S3-S4 is parallel to the membrane for tilting angles greater than 60°).

(c) The shortest distance between atoms in S1-S2 to atoms in S3-S4 of the same subunit should be smaller than 10.0Å (for a distance beyond 10.0Å, S3-S4 is no longer packed with S1-S2 and the interactions between charged residues on S2 and S4 are weak).

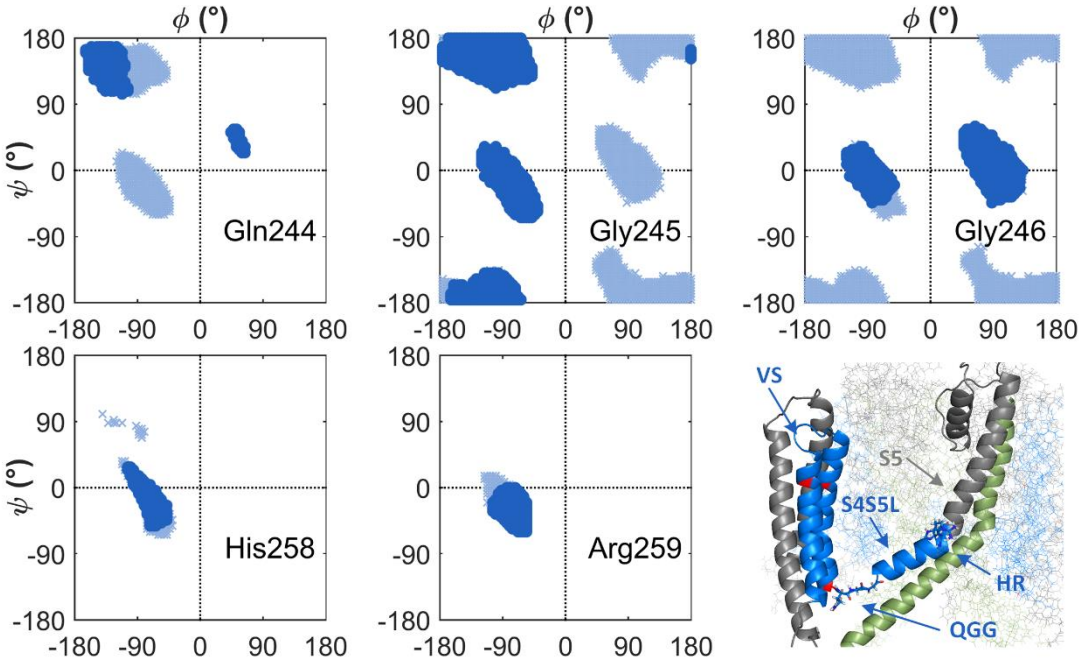

Figure 2.3, Ramachandran plots of the residues with dihedral angles that were varied to construct the VSL library; the VSL is shown in the bottom right panel as S1-S2 in grey and S3-S4-S4S5L in blue (see also Figure 2.1D). In the Ramachandran plots, light blue marks the initial possible dihedral angles subject to constraint (a) in Section 2.3.2. Dark blue marks the final region of possible structures after application of constraints (b) to (f) in Section 2.3.2. VS, voltage sensor; QGG, Gln244-Gly245-Gly246; HR, His258-Arg259; other abbreviations and color codes are the same as in Figure 2.1.

(d) The side-chains in a VSL conformation should be well packed within the conformation and with the static S5 segments. In application of this constraint, S1, S2 and S3 were released and allowed to move within 1.0Å RMSD to prevent steric clashes.

(e) For a given VSL conformation, there should be more than 0.1% conformations in the pore library that do not have steric clashes with the VSL.

(f) The conformation could be reached from the starting conformation through small (<1.0Å) conformational changes.

The final VSL library included 11,547,630 conformations. The mean z value of the C_α atoms of Arg228 in S4 and Val212 in S3 was calculated to represent the translation of the VS across the membrane. The rotation angle of VS about the z-axis (ω) was computed using the vector from C_α of Val212 to C_α of Arg228. The angle between the vector from C_α of Arg243 to C_α of Arg228 and the z-axis was used to compute the VS tilt (γ).

2.3.3. The KCNQ1 Tetramer Library

A complete KCNQ1 conformation was composed of four VSL domains and one pore. Each of the four VSL domains could assume any conformation from the VSL library. The pore was not permitted to have steric clashes with any of the VSL domains. There were more than 10^{30} possible KCNQ1 structures. To avoid storing all tetramer structures, only a correlation vector was calculated and stored. This vector indicated all conformations in the pore library that could assemble with a given VSL conformation. A subset of the complete KCNQ1 library was chosen as a sample set with four symmetric VSL domains in the tetramer and a coarse grid (2.0Å~3.0Å RMSD compared to 0.3Å~0.5Å for the full library). This subset was selected to cover the full range of VSL translations and rotations and the entire range of pore diameters in the complete library.

2.4. IKs Structural Library

The space occupied by KCNQ1 was estimated using the sample set of the KCNQ1 library in the coarse-grid discretized space. A volume element was considered occupied by a KCNQ1 conformation if it was located within the van der Waals radius of one atom in the conformation. In the initial docking procedure, KCNE1 was allowed to dock in a volume element that was occupied by less than 90% of KCNQ1 structures in the sample library. The KCNQ1 transmembrane domain creates four pockets between adjacent voltage sensor domains (Figure 2.4; brown stars). Two KCNE1 transmembrane segments were docked into two opposite pockets in a KCNQ1 conformation to construct IKs.

Starting with NMR data (PDB: 2K21) [Kang 2008, Sahu 2014, Sahu 2015], the template for the transmembrane segment of KCNE1 was refined in a membrane-water box by a NAMD simulation [Phillips 2005]. The potential docking positions and orientations of KCNE1 in the system were generated by shifting the template to different positions in the x-y plane with various degrees of rotations about the z-axis and of tilting angles from the z-axis (Figure 2.5). The grid of translations was 0.5 Å. The grid of rotations was 15° from 0 to 345° and tilting was from 0 to 30° at 5° increments. The library of possible KCNE1 structures was limited by the available docking volume estimated in Figure 2.4. This resulted in 7,448 acceptable conformations. For each KCNQ1 conformation, the docking site of KCNE1 was then refined by imposing the following constraints:

(a) Steric clashes between backbone atoms of KCNE1 and KCNQ1 cannot occur.

(b) Interacting KCNE1-KCNQ1 residues (Table 2.2) should be located sufficiently close (< 12.0 Å between their C_α atoms).

(c) Side chains of the KCNE1-KCNQ1 protein should be well packed for the selected KCNE1 conformation.

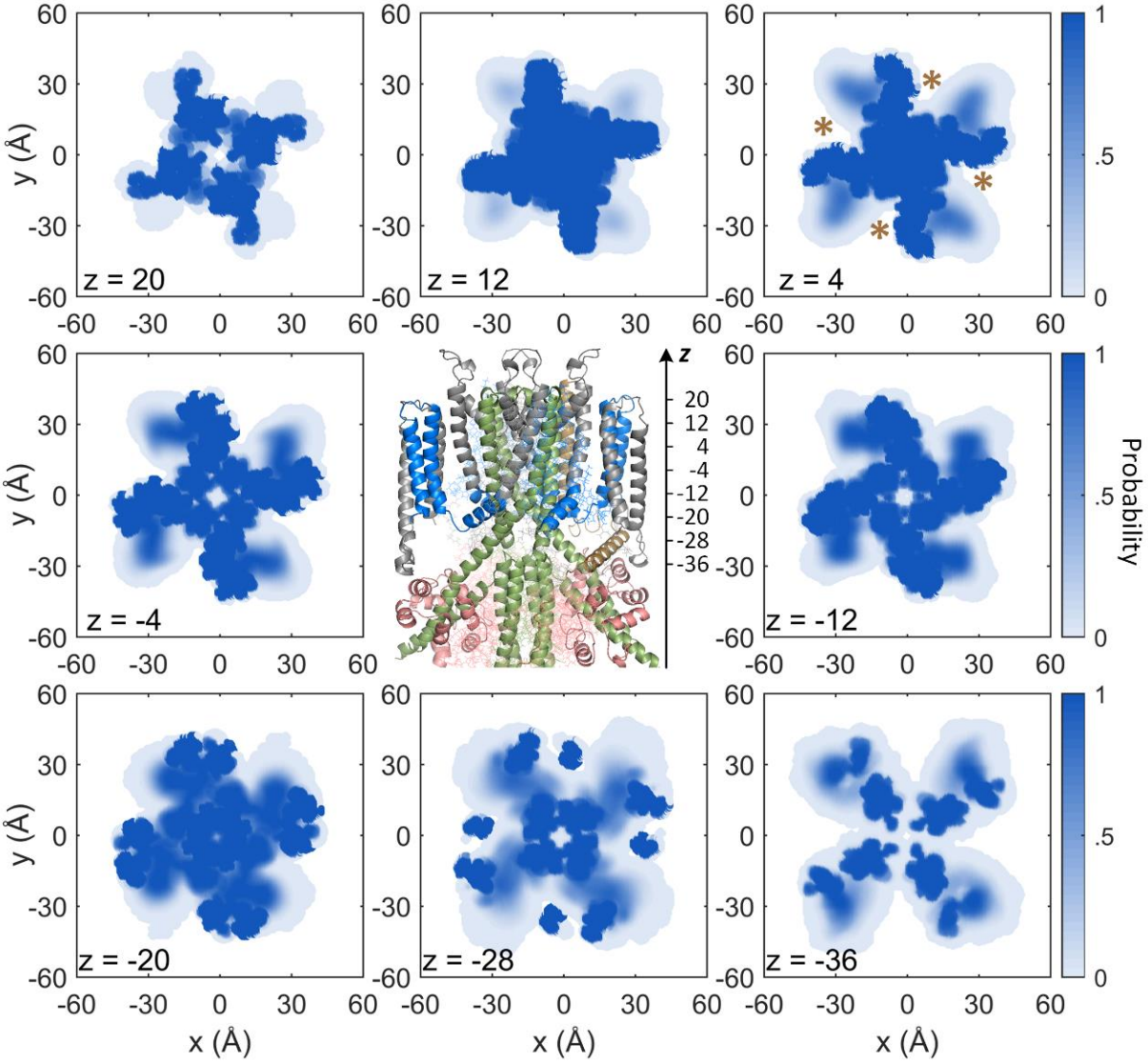

Figure 2.4, Probability of volume occupation by KCNQ1. A KCNQ1 structure is shown in the center as reference. Each panel shows an x-y plane at a different height z. Brown stars indicate docking pockets for KCNE1. In the initial step of the docking procedure, the volume with probability less than 0.9 of occupation by KCNQ1 was considered available for KCNE1 docking.

Table 2.2. KCNE1 residues that interact with KCNQ1 residues based on experimental data

KCNE1 residues	KCNQ1 residues	Experiment
Gly40/Lys41	Ile145 adjacent to S1 C-terminus	Cys substitution [Wang 2011]
Lys41/Leu42	Ile145; Val324 (S6)	Cys substitution [Chung 2009]
Phe54/Gly55	Cys331 (S6)	Cys substitution [Tapper 2011]
Thr58	Phe339 (S6)	Ala scanning [Strutz-Seebohm 2011]
Thr58	Phe340 (S6)	Double mutation [Panaghie 2008]
Thr58	Ala341 (S6)	Double mutation [Mikuni 2011]
His73/Ser74	Ile257 (S4-S5 linker)	Cys substitution [Lvov 2010]

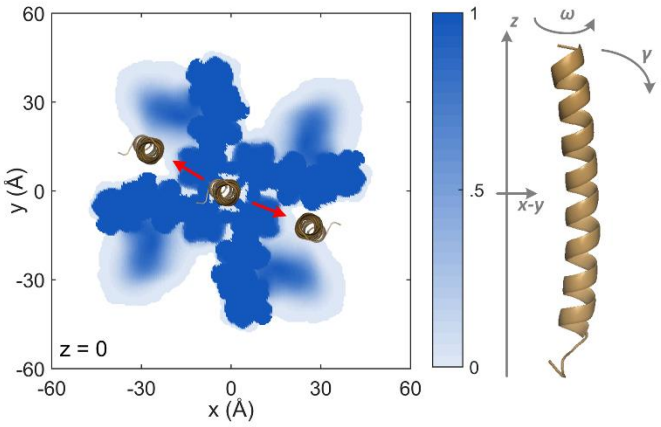

Figure 2.5, Translation (red arrows) and rotation of KCNE1 (brown) in the coordinate system shown on the right. Blue scale shows KCNQ1 occupation at z = 4.

2.5. Electrostatic Energies

The KCNQ1 or IKs conformations were inserted into a 140Å x 140Å x 140Å lipid-water box. The center of the membrane (POPE) was aligned to the x-y plane at z = 0. A PIP2 molecule was docked at the lipid-water interface near S4S5L. An energy component analysis of a coarse-grid sample KCNQ1 library (40,490 conformations) equilibrated by NAMD was conducted to validate the assumption [Rudy 2006] that electrostatic interactions play a dominant role during channel gating, even at zero membrane voltage (Figure 2.6A). The electrostatic energy

of each conformation in the library was computed using the Generalized Born equation [Still 1990, Im 2003],

$$E_{GB} = \frac{-1}{2}\left(\frac{1}{\varepsilon_p} - \frac{1}{\varepsilon_w}\right)\sum_{i,j}\frac{q_i q_j}{\sqrt{r_{ij}^2 + \alpha_i \alpha_j exp\left(-r_{ij}^2/4\alpha_i\alpha_j\right)}} \qquad (2.2)$$

where the dielectric constant of the protein and membrane ε_p = 2.0, the dielectric constant of water ε_w = 80.0, i and j are the indices of atoms in the protein, q_i and q_j are the charges, r_{ij} is the distance between the atoms and α_i and α_j are the effective Born radii of the atoms. To overcome the intense computation requirement for computing the Born radii of all atoms in each conformation, a test was performed on the coarse-grid sample KCNQ1 library. The Born radii of atoms in the entire protein vary by less than 4.6% over the sample set, except for atoms on S3, S4 and S4S5L which could vary by 8.9% (Figure 2.6B). This larger variation could be caused by significant shifts of the S3, S4 and S4S5L between the membrane and water phases. However, the effective Born radii of atoms in different conformations were similar if their z coordinates were similar. Thus, to calculate the electrostatic energy for the entire library, the effective Born radius for an atom in S3, S4 and S4S5L at a certain z was assigned its value in a conformation of the sample set with the closest z position (the difference in z was always smaller than 0.2Å). The mean values across the sample set were used to approximate the effective radii of all the other atoms. The electrostatic energy of a KCNQ1 conformation in the membrane-water environment was computed with one equilibrated membrane-water box selected from the sample set with the smallest RMSD to the target. Calculations for the IKs sample library provided effective radii that were different from those for the KCNQ1 library, but with a similar variation across the library. The radii for KCNE1

atoms do not vary by more than 4.0% and the mean values for the sample library were used. The non-linear term α in equation (2.2) was a constant or obtained from a lookup table.

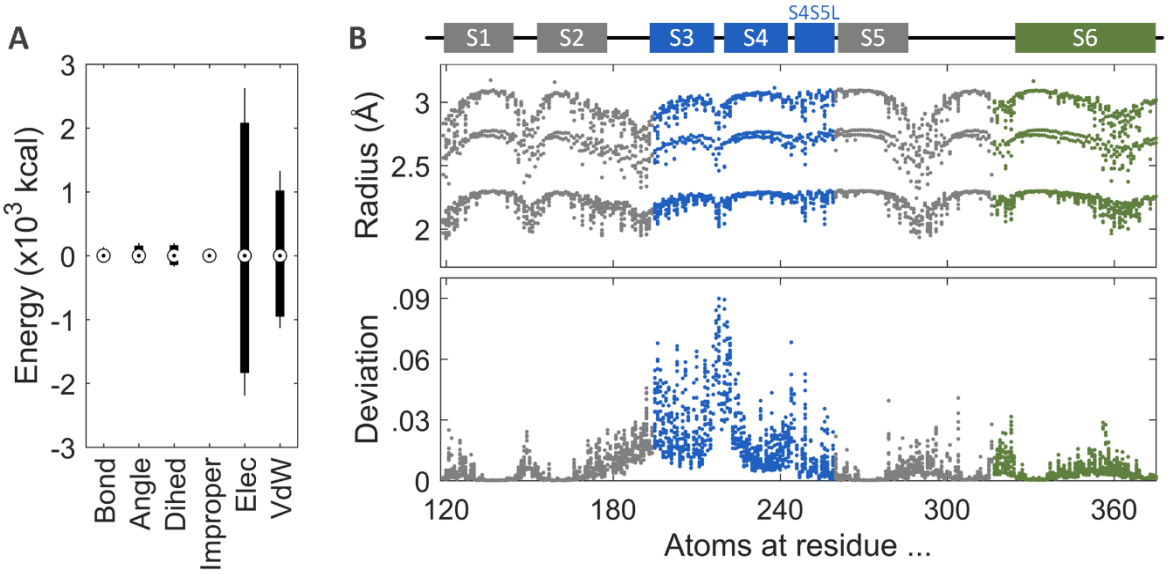

Figure 2.6, (A) Variance of energy components in conformations across a coarse-grid library subset, in a lipid-water box: bond, angle, dihedral (dihed), improper, electrostatic (elec) and van der Waals (VdW) interactions. All the components are aligned to their median values and the range across the library (5% to 95% of maximum) is depicted by the black bars. Note the dominant contribution from electrostatic energy and significant contribution from van der Waals energy. (B) Top: Mean effective Born radii of KCNQ1 atoms estimated in the library subset. Bottom: Deviations of estimated radii across the subset. Note the relatively large deviations for atoms in S3, S4 and S4S5L compared to all other atoms of the protein.

To improve the computation efficiency of the Generalized Born equation for the large conformation library, the complete protein structure was considered as an assembly of different domains: VSL, Pore and KCNE1 (Figure 2.7). Using the linearized Born equation, the total Born energy, E_{GB}, could be computed using superposition of individual contributions as

$$E_{GB} = \sum_i E_i + \frac{1}{2}\sum_{i \neq j} E_{i,j} \qquad (2.3)$$

where E_i is the Born energy of element i and $E_{i,j}$ is the interaction term between two elements. Interactions between opposite chains were neglected due to the large distance between them.

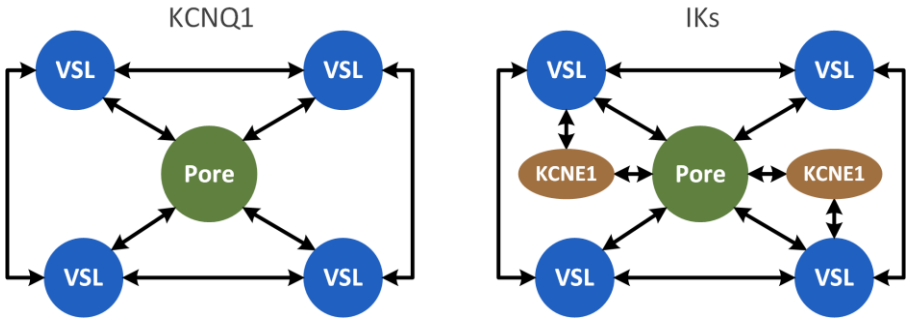

Figure 2.7, Schematics identifying the structural components to which the protein was divided for library construction and energy computations; the arrows indicate electrostatic interactions that were included in energy computations in addition to the self-energy contribution of each component. The protein segments that comprise these structural components are shown in the color-coded cartoon in Figures 1.2 and 2.1.

At a membrane voltage V_m, the total protein energy of a conformation, E_{elec}, was calculated as

$$E_{elec} = E_{GB} + \sum_i E_{v,i} \qquad (2.4)$$

where $E_{v,i}$ is the energy of atom i in the electric field created by the voltage V_m across the membrane

$$E_{v,i} = \begin{cases} 0, z_i \leftarrow \frac{1}{2} z_m \\ -q_i \int_{\frac{-1}{2} z_m}^{z_i} \frac{V_m}{z_m} dz, -\frac{1}{2} z_m \leq z_i \leq \frac{1}{2} z_m \\ -q_i \int_{\frac{-1}{2} z_m}^{\frac{1}{2} z_m} \frac{V_m}{z_m} dz, z_i > \frac{1}{2} z_m \end{cases} \qquad (2.5)$$

and the thickness of the membrane z_m = 30.0 Å.

Note that all-atom van der Waals interactions were also incorporated in the total energy to compute the trajectories below.

2.6. Trajectories of Conformational Changes During Activation

Conformational changes of the KCNQ1 or IKs protein during activation were simulated by its movement in conformational space across the conformation library, driven by a gradient on the electrostatic energy landscape [Silva 2009]. With assumption of a Boltzmann distribution, the probability of being with a conformation C_i at time t was calculated by Smoluchowski equation [Ansari 2000] as

$$\frac{\partial p(C_i,t)}{\partial t} = \sum_{j\neq i} k(i|j)p\big(C_j,t\big) - p(C_i,t)\sum_{j\neq i} k(j|i) \qquad (2.6)$$

where the rate constant, k(i|j), for making a transition from C_i to C_j within the time step (Δt) is defined by

$$k(i|j,\Delta t) = e^{-\left(E_{elec,i}-E_{elec,j}+F\left(C_i\rightarrow C_j,\Delta t\right)\right)/2k_BT} \qquad (2.7)$$

where $E_{elec,i}$ is the electrostatic energy of conformation C_i calculated by equation (2.4), k_B is the Boltzmann constant (0.001987 kcal/(mol·K)) and temperature T = 298.15K (25°C). To include the resistance of the environment to significant movement of the protein, a friction term [Nekouzadeh 2011] was introduced in the calculation as

$$F\big(C_i \rightarrow C_j,\Delta t\big) = f\frac{m_p RMSD_{C_i\rightarrow C_j}}{\Delta t} \qquad (2.8)$$

where m_p is the mass of the protein (124.50 kg/mol for KCNQ1 and 132.53 kg/mol for IKs), $RMSD_{C_i\rightarrow C_j}$ is the root mean square deviation between the two conformations and the empirical friction constant f = 3.5160×10^{-12} kcal·s/(kg·Å). Starting conformations were randomly chosen from the structural library of KCNQ1 or IKs. The following conformations were chosen by a random walk process, with conformations weighted by equation (2.6). Conformations far away

structurally from the previous conformation ($RMSD_{C_i \to C_j} > 5.0$Å) were neglected due to the small probability.

The following protocol was used to activate the channel: after 18 seconds at holding potential of -80mV, the membrane potential was changed to voltages from -140mV to +100mV in steps of 20mV and held for more than 10 seconds. 2000 trajectories of KCNQ1 or IKs were generated to simulate the conformational changes of 2000 independent channels during each protocol. The macroscopic (ensemble) behavior of KCNQ1 and IKs was calculated as the average values of z, ω, γ, D_{pore} and Pc over 2000 trajectories. The time dependence of macroscopic activation traces was characterized using a double-exponential-component analysis. The time step Δt in equation (2.6) was scaled to 0.3695 ns based on the ratio between the estimated fast time constant and that measured in experiments [Nakajo 2014].

2.7. Macroscopic IKs Current During the Action Potential in Whole-Cell Model

The voltage dependence and time constants of the macroscopic Pc traces were integrated into a human ventricular myocyte model [O'Hara 2011] to simulate the effects of KCNQ1-KCNE1 interaction on the action potential. In [O'Hara 2011], IKs is formulated as

$$I_{Ks} = \overline{G_{Ks}} \cdot \left(1 + \frac{0.6}{1 + \left(\frac{3.8 \times 10^{-5}}{[Ca^{2+}]_i} \right)^{1.4}} \right) \cdot x_{s1} \cdot x_{s2} \cdot (V - E_{Ks}) \qquad (2.9)$$

and used to compute current during the AP. To introduce results from the structural simulations, the activation gates (x_{S1} and x_{S2}) were recalculated using the magnitudes and time constants of the

Pc trajectories at different voltages. For KCNQ1, steady state values and time constants for x_{S1} and x_{S2} were computed as

$$x_{s1,\infty} = x_{s2,\infty} = \frac{1}{1 + e^{-(V+11.79)/15.93}} \qquad (2.10)$$

$$\tau_{s1} = 346.5 + \frac{1}{0.001908 \times e^{(V-85.43)/77.44} + 0.01812 \times e^{-(V+146.1)/39.79}} \qquad (2.11)$$

$$\tau_{s2} = \frac{1}{0.01129 \times e^{(V-91.05)/80} + 0.05978 \times e^{-(V+85.84)/25.44}} \qquad (2.12)$$

And the equations for IKs were

$$x_{s1,\infty} = x_{s2,\infty} = \frac{1}{1 + e^{-(V-15.05)/19.72}} \qquad (2.13)$$

$$\tau_{s1} = 712.6 + \frac{1}{0.001 \times e^{(V-96.93)/49.61} + 0.001029 \times e^{-(V+168.4)/209.3}} \qquad (2.14)$$

$$\tau_{s2} = \frac{1}{0.002757 \times e^{(V-96.29)/80} + 0.05744 \times e^{-(V+82.33)/20}} \qquad (2.15)$$

The maximum conductance of IKs, $\overline{G_{Ks}}$, was estimated at 0.0399mS/µF using an AP-clamp protocol, so that the total charge carried by IKs in one cycle (CL = 1000ms) was the same as in the O'Hara model. For KCNQ1, $\overline{G_{Ks}}$, was adjusted to 0.0060mS/µF through multiplication by the ratio between its maximum open probability (maximum Pc) and that of IKs. Isoproterenol (ISO) effect on IKs was incorporated by multiplying $\overline{G_{Ks}}$ by a factor of 3 [Heijman 2011].

Chapter 3 Results and Discussion

3.1. Structural Properties of the Conformation Space

To study the dynamic conformational changes of the transmembrane domain of KCNQ1 during channel activation, we constructed an all-atom structural library of this domain with the proximal C-terminal segments attached. Following elimination of structures through application

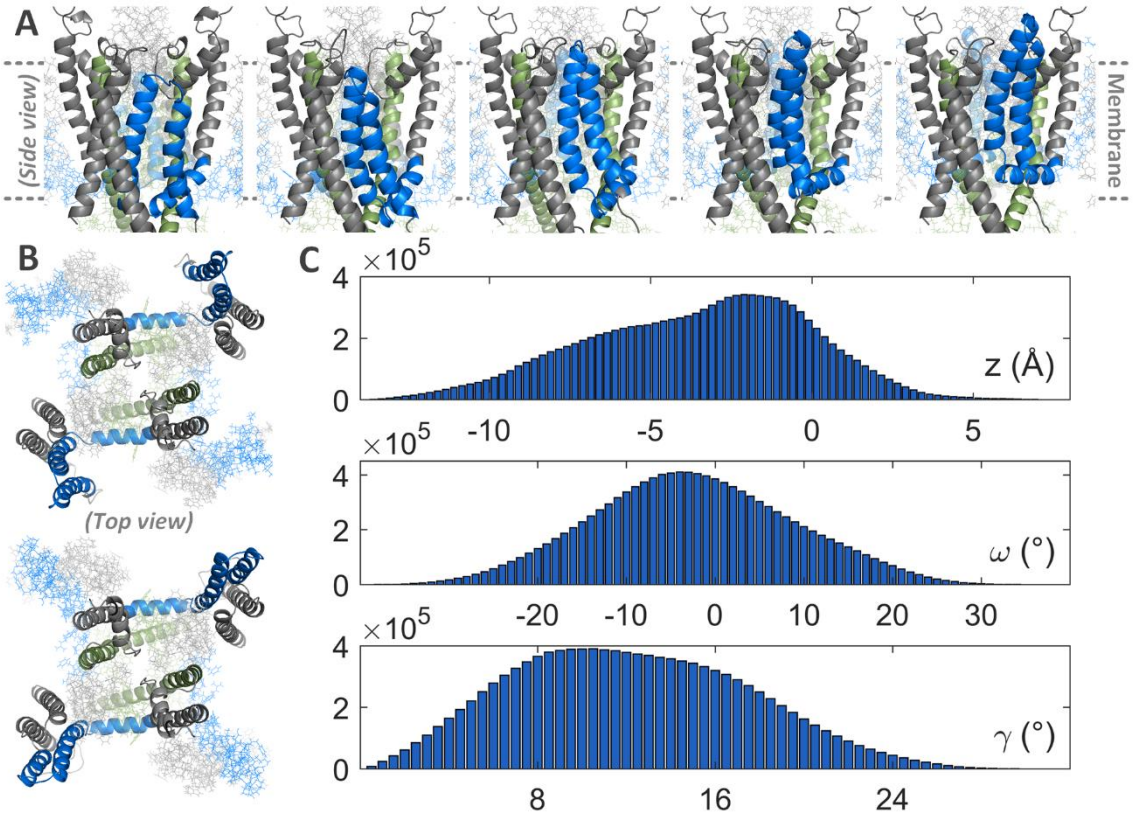

Figure 3.1, (A) Selected KCNQ1 conformations from the structural library with VS from low z to high z (left to right). Only one KCNQ1 subunit is shown; S3-S4 and S4S5L are in blue. (B) Two KCNQ1 conformations with different rotation angles of VS on the x-y planes (top view) are shown, with their selectivity filters aligned. (C) Distribution of VSL conformations across the structural library, shown with three structural parameters. Top to bottom: VS z position (translation); rotation of VS about its own z axis (ω); tilting of VS relative to z axis (γ). The y-axis is number of conformations.

of spatial constraints and minimization of van der Waals energies, the library retains 11,547,630 VSL conformations and 615,946 pore conformations, which amounts to more than 10^{30} possible KCNQ1 structures. In the library, the spatial range of the S1-S2 panel is limited to 2Å. The S3-S4 paddle can translocate 22.01Å in the z direction across the membrane, rotate about the z-axis (ω) within a range of 79.08° and tilt (γ) relative to the z-axis from 0 to 32.24° (Figure 3.1). The C-terminal half of S6, together with the proximal cytosolic domain, can swing around an axis through the center of the pore, allowing the pore diameter to change over a range from 0 to 15.85Å (Figure 3.2). The library includes conformations of Helix A-Helix B-Calmodulin that occupy a volume consistent with (less than 0.3% difference) from that in a recently published cryo-EM structure of KCNQ1 [Sun 2017]. When VSL locates at high z positions (H-VSL, top panel in Figure 3.3A), considered an activated state of the voltage sensor, it is possible to have structures with open or closed pore conformations. It is not necessary that all four VSLs be activated for the pore to be open; a subset of permissible open pore conformations have VSLs at low z positions (L-VSL, bottom panel in Figure 3.3A). Thus, the KCNQ1 channel can have a conducting (open) pore with some or even all voltage sensors at low positions. Importantly, some combinations of four H-VSLs can assemble with up to 68% of the open pore conformations without steric clashes, compared to only 18% for four L-VSLs. This results in a greater probability for the channel to be in a conducting state when more VSLs are at high positions.

3.2. Effect of Membrane Potential

Based on computed energy landscapes of the structural library, the VSLs favor different clusters of conformations at different membrane potentials, consistent with experimental observations [Zaydman 2014]. At resting potentials (−80mV in Figure 3.3B), VSLs reside

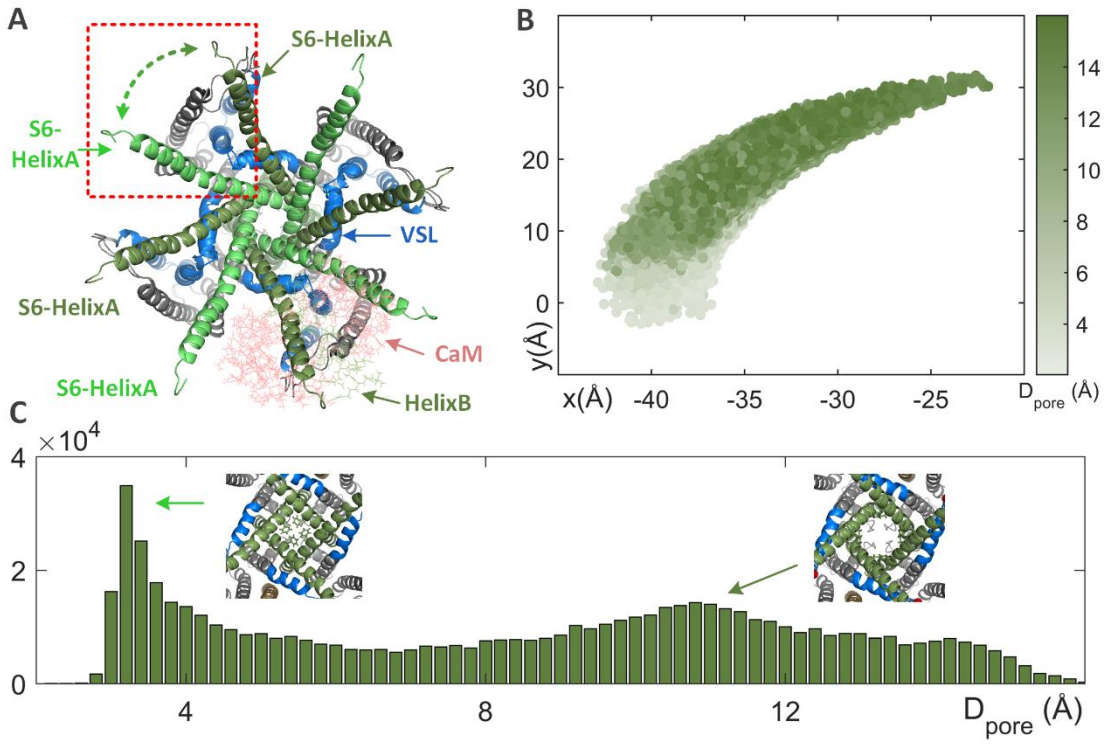

Figure 3.2, Conformational space of pore-forming S6-HelixA segments and relationship between S6-HelixA conformations and pore diameter. Labels are color coded to structures. (A) Bottom view of two superimposed KCNQ1 conformations with the same VSL but different pores. The pore conformation in light green has a diameter smaller than that in dark green. The dashed arrow between two S6-HelixA structures shows the conformational space of the pore domain for the particular VSL conformation shown (blue). Only one CaM and one Helix B are shown with thin lines, to indicate the entire spatial occupation by the cytosolic domain of one KCNQ1 subunit. Red box approximates the x-y box of panel B. (B) Possible locations of the C-terminal tail of S6-HelixA of one KCNQ1 subunit in the x-y plane and associated pore diameter (D_{pore}, green color scale). The direction out of the paper is towards the cytosolic medium. (C) Distribution of pore conformations across the structural library, shown with D_{pore}. Two structures with different pore domains are shown as examples.

preferentially at low z positions, where R228 and R231 on S4 can form salt bridges with E160 on S2, and R237 on S4 is close to E170 on S2 (L-VSL). Following depolarization (+60mV in Figure 3.3B), there is an increased probability for VSLs to translocate in the positive z direction, to conformations where R237 is closer to E160 (H-VSL). Hence, at depolarized potentials there is greater probability for VSLs to be in the activated state and for the pore to be open (conducting).

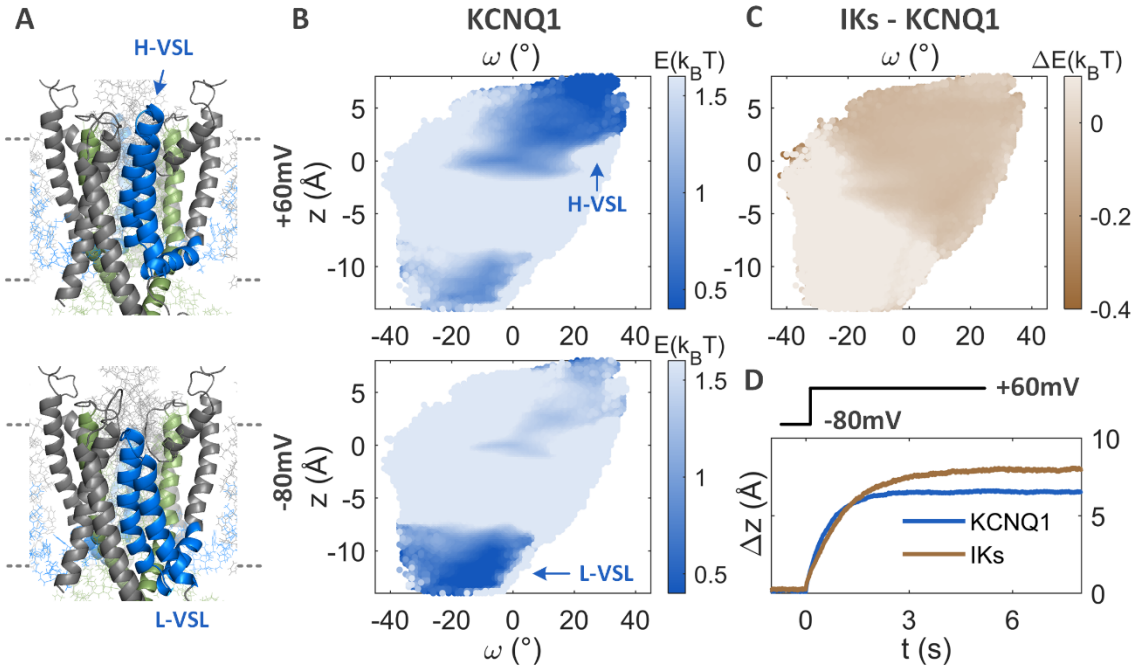

Figure 3.3, (A) Two KCNQ1 conformations selected from the library with VSL at high z (top, H-VSL) and low z (bottom, L-VSL). Dashed lines mark the membrane boundaries. (B) Energy landscapes for VSL in KCNQ1 across the structural library at -80mV (bottom) and +60mV (top). Arrows indicate the corresponding z positions for each representative conformation in panel A on the energy landscape. There is lower energy (hence preferred residency) in low z and small ω at -80mV, and high z and large ω at +60mV (dark blue). (C) Difference energy landscape (IKs – KCNQ1) at +60mV reveals preferential residency in high z and large ω conformations of IKs compared to KCNQ1. (D) VSL trajectories in z coordinate for KCNQ1 (blue) and IKs (brown), during step depolarization (shown on top).

Note that the energetically favored z positions of VSL at resting and depolarized potentials are less than 12Å apart. This distance is much smaller than the permissible range of 22Å (space unoccupied by other protein segments); it is consistent with the range predicted experimentally for the voltage sensor movement of Kv1.2 [Tombola 2005]. In addition to the z translocation, the energy landscape indicates that VSLs favor conformations with different ω-rotation at different voltages (Figure 3.3B).

To simulate KCNQ1 activation gating, we computed trajectories of conformational changes in response to membrane depolarization to different voltages. When the membrane is depolarized to +60mV, 1.7% to 2.1% of the KCNQ1 channels became activated with high VSL conformations and large pore diameter (+60mV trace in Figures 3.4A and 3.5). The trajectories maintained tight coupling between VSLs and pore, a property that underlies KCNQ1 fast activation without substantial delay. The average z position of VSLs and open probability of the channel (Pc) share a similar voltage dependence (Figure 3.6A, top) and the fast and slow time constants of Pc follow the time constants of VSL translocation in the z direction (Figure 3.6B). This behavior, indicative of a tight VSL-pore coupling in KCNQ1 channels, is consistent with voltage-sensor fluorescence experiments [Osteen 2010, Nakajo 2014].

3.3. Modulation of KCNQ1 Activation Gating by Co-assembly with KCNE1

A stoichiometry of 4KCNQ1:2KCNE1 is considered the physiological stoichiometry of IKs [Plant 2014]. The structural library of IKs was generated by inserting into each tetrameric KCNQ1 conformation two KCNE1 subunits in opposite positions (Figure 2.1C). Docking of KCNE1 does not eliminate any possible conformations in the KCNQ1 library, as the single-spanning transmembrane helix of KCNE1 occupies less space than the empty pocket between the voltage sensors from two adjacent KCNQ1 subunits (Figures 2.4 and 2.5). However, charges carried by KCNE1 residues change the electrostatic energy landscape of KCNQ1 (Figures 3.3 and Figure 3.7) and consequently the steady-state z-position, ω-rotation and γ-tilt of VSL at resting and depolarized potentials (Figures 3.4, 3.5 and 3.7). KCNE1 makes H-VSLs energetically more favorable at depolarized voltages, so that IKs achieves a higher average z of VSL and a larger open

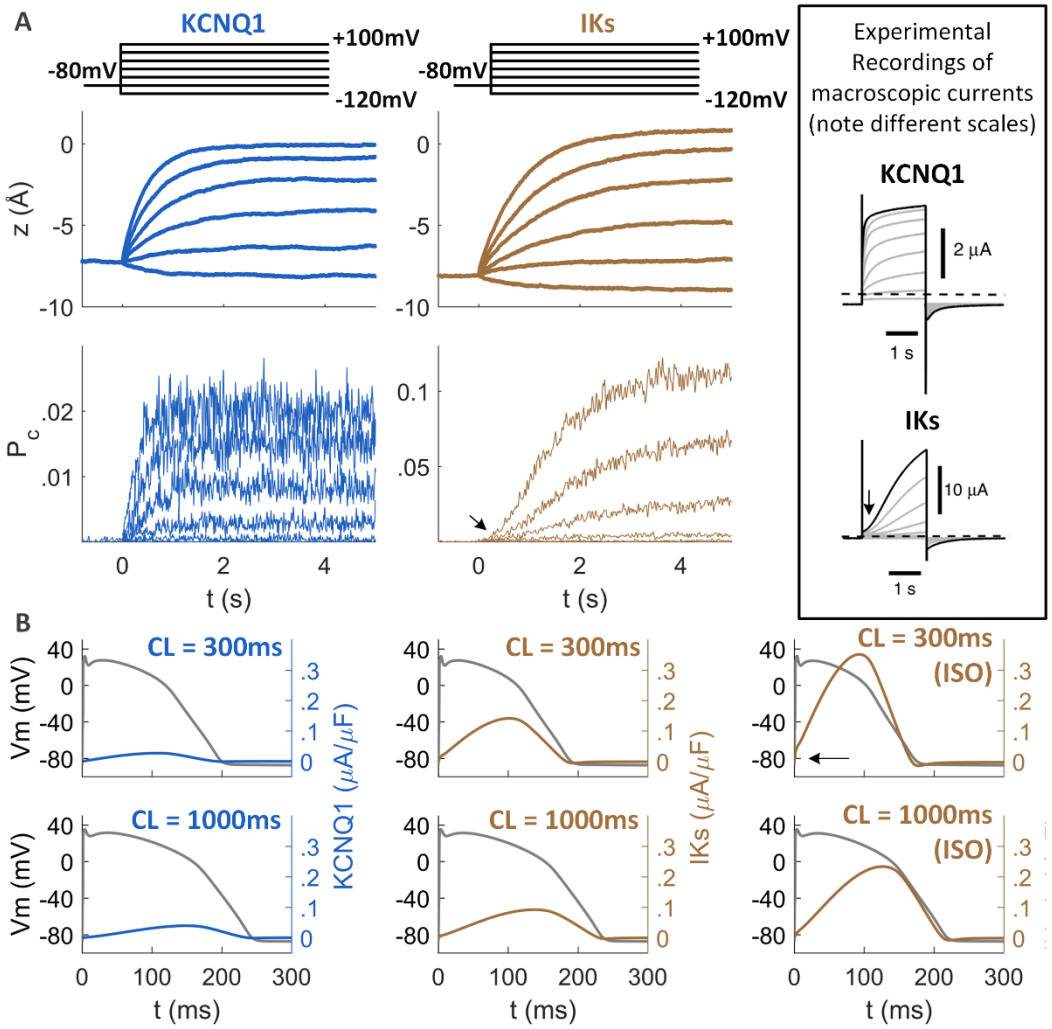

Figure 3.4, (A) Conformational changes of KCNQ1 (left) and IKs (right) in response to a depolarizing step (protocol on top). Traces show VSL z position (top) and estimated probability for the channel to be in a conducting state (Pc, bottom). The stochasticity of conformational changes is reflected in the fluctuations of Pc. Experimental recordings of these currents, for a similar protocol, are shown in the framed panel (right [Nakajo 2014]). Note the 5-times greater magnitude of computed IKs Pc and of recorded IKs compared to KCNQ1 (shown with different scales). The simulated delayed activation of IKs (arrow in the IKs Pc panel) reproduces the delay in the recorded IKs current (arrow in the framed panel). (B) Macroscopic currents during a human ventricular AP [O'Hara 2011] paced at two rates: top panels CL = 300ms, bottom panels CL = 1000ms. Left panels: KCNQ1. Middle panels: IKs without ISO. Right panels: IKs with ISO. The currents are computed using the Pc of panel A, which, in turn, is computed from the protein structural changes during activation. Note current accumulation with ISO at fast rate (arrow in the top right panel). Traces in the framed inset are reproduced from [Nakajo 2014]. ISO, isoproterenol.

probability compared to KCNQ1. The computed Pc traces (Figure 3.4; note different scales of panels) for IKs are 5 times larger than for KCNQ1, as observed in experiments [Sanguinetti 1996, Osteen 2010, Nakajo 2014, Barro-Soria 2014]. However, conformational changes of IKs are slower to reach steady state (Figure 3.4). The co-expression of KCNE1 with KCNQ1 separates the voltage and time dependence of VSL z translation from that of pore opening (Figure 3.6), reducing

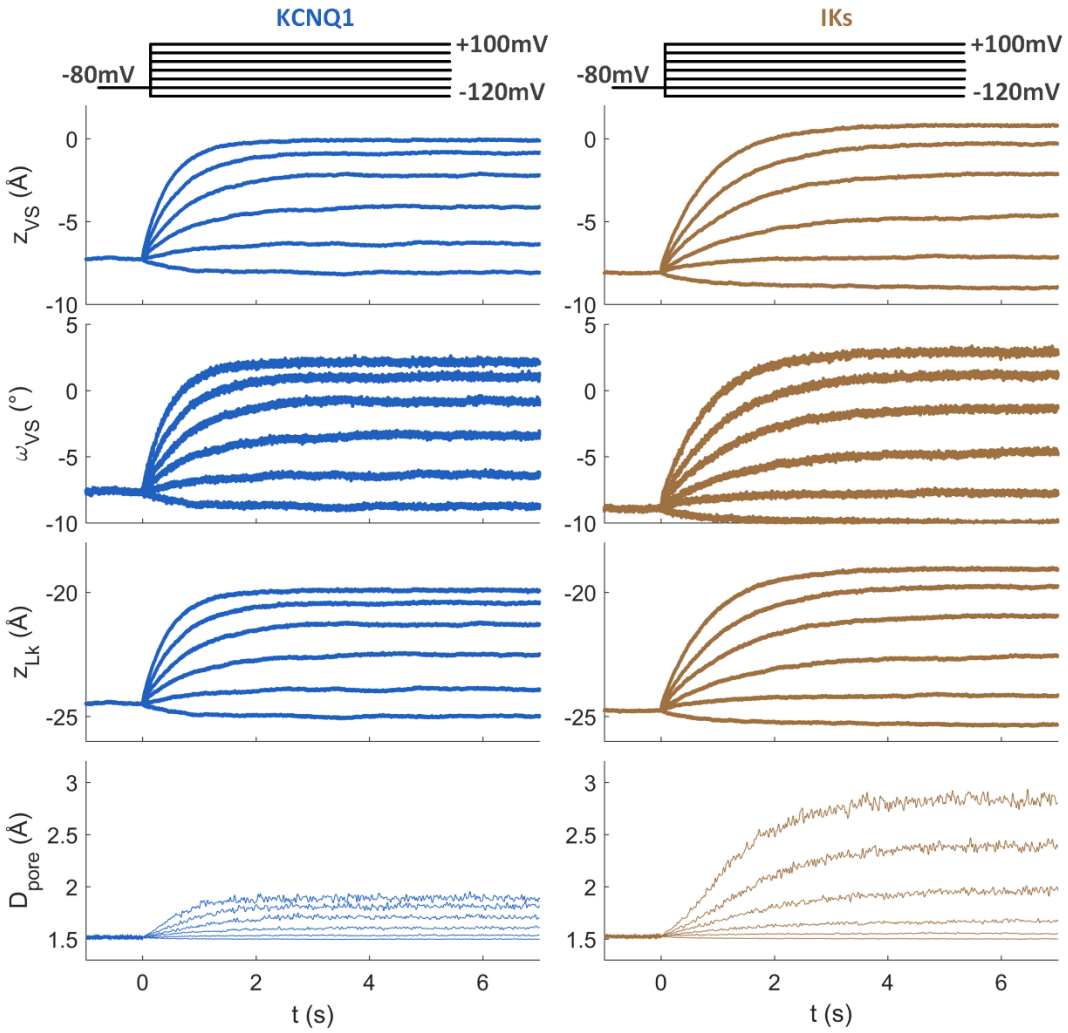

Figure 3.5, Conformational changes of KCNQ1 (left) and IKs (right) in response to the depolarization protocol shown on top. Only 40mV steps are shown for clarity. The four rows show (top to bottom) average changes of VSL in z-translation (z_{VS}), ω-rotation (ω_{VS}), z-translation of S4S5L (z_{Lk}) and pore diameter (D_{pore}). At a depolarized membrane voltage, steady-state z_{VS} and z_{Lk} are higher for IKs than KCNQ1, and ω_{VS} is smaller. D_{pore} is large for IKs. These conformational changes are significantly slower for IKs compared to KCNQ1.

the coupling between these two motions. The simulations (Figure 3.6) reproduce experimental measurements [Osteen 2010, Nakajo 2014], except at low membrane voltages (Vm = −60mV and −40mV for $\tau_{Z,VS}$ of KCNQ1 and Vm = 20mV and 40mV for τ_{Pc} of IKs) for which the experimentally recorded signals are too small to separate multiple temporal components. Comparison between the simulated KCNQ1 and IKs trajectories shows that at resting membrane potentials, VSLs of IKs reside at lower z positions at steady state, but translocate to higher z upon

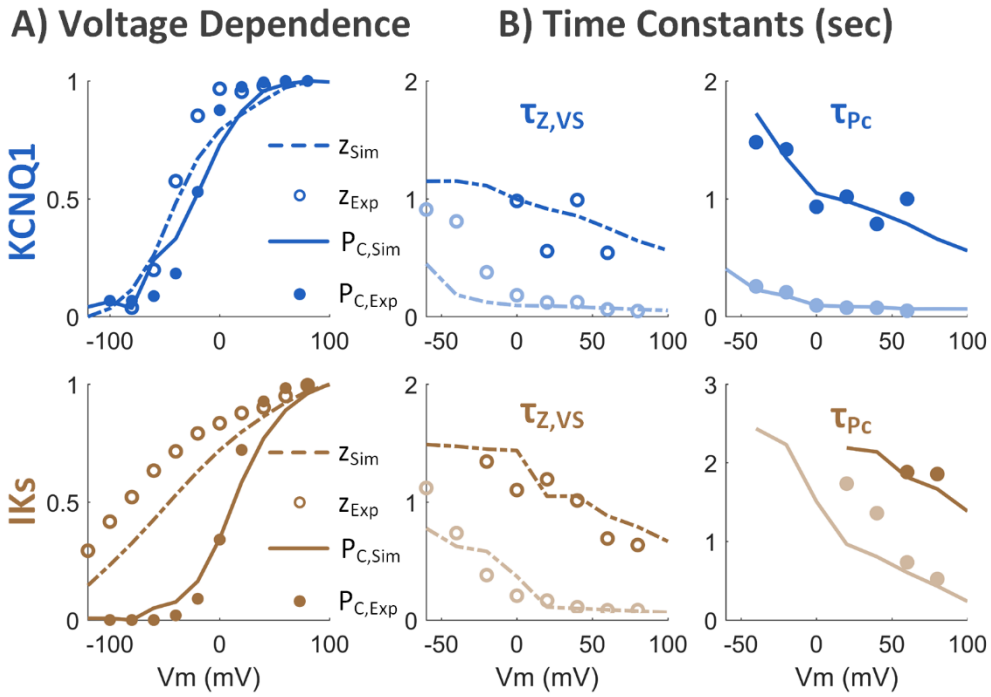

Figure 3.6, Quantitative comparison between simulations (line traces) and experimental recordings (symbols) for the protocol in Figures 3.4 and 3.5. (A) Normalized voltage dependence of VS z translation (dashed line) and conducting-state probability of the channel (Pc, solid line) of KCNQ1 (top, blue) and IKs (bottom, brown). Note separation of z and Pc voltage dependence in IKs but not KCNQ1. (B) Time constants of z (left) and Pc (right) for the same protocol; light or dark color represents fast or slow time constant, respectively. Note the different τ_{Pc} scale in the bottom right panel, reflecting a large increase of the fast time constant (slowing) for pore opening in IKs, compared to KCNQ1. Experimental recordings are from [Nakajo 2014]; empty circles are fluorescent signals of voltage sensor movement; filled circles are recorded macroscopic current.

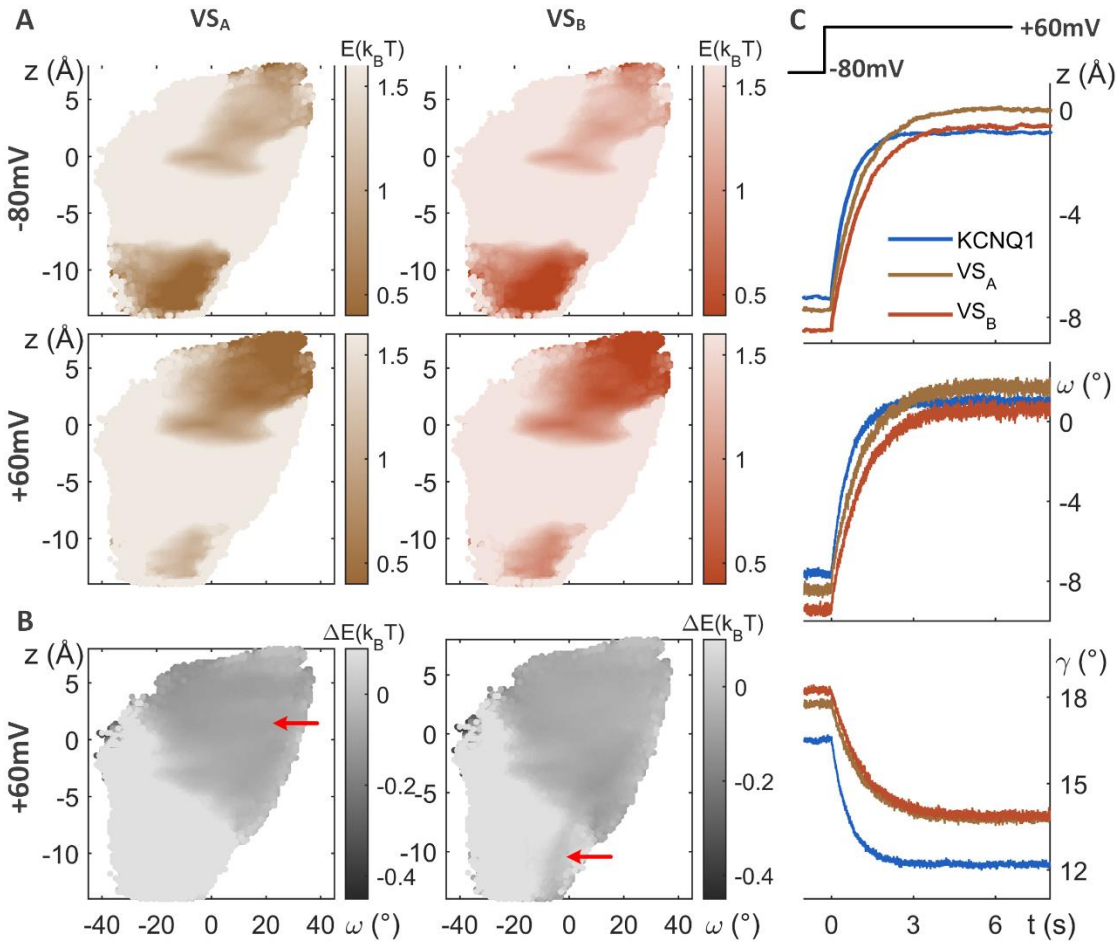

Figure 3.7. Differences between two types of VSLs in IKs in terms of energy landscapes and conformational changes during activation. (A) Electrostatic energy landscapes of VS_A (left) and VS_B (right) at -80mV (top) and +60mV (bottom). VS_A and VS_B share preference for similar conformations at the resting and depolarized potentials, with minor differences. (B) Difference energy landscape between VS_A (left) or VS_B (right) and KCNQ1 at +60mV. Both VS_A and VS_B have greater preference for high-z VSL conformations (H-VSL) than VS of KCNQ1. (C) VSL trajectories in z (top), ω (middle) and γ (bottom) dimensions for VSL of KCNQ1 (blue), VS_A (brown) and VS_B (red) upon a step depolarization (shown on top). KCNE1 changes the electrostatic energy landscapes of VS_A and VS_B in different ways, leading to different trajectories. At +60mV, H-VSL is more preferred in the VS_A library (area pointed to by the red arrow in panel B, left) and the VS_A trajectory achieves a higher z position at steady state compared to KCNQ1. In contrast, the VS_B trajectory starts at a lower z and reaches a similar z to KCNQ1. The reduced probability for H-VSL in the VS_B library is due to another preferred cluster of structures with L-VSL that compete with the energetically favored H-VSL (indicated by the red arrow in panel B, right). H-VSL and L-VSL are defined in the text.

depolarization. This prolongs the time to steady-state following depolarization of IKs compared to KCNQ1. However, more IKs channels accumulate in conformations with larger pore diameters at a depolarized steady state (Figure 3.8), accounting for the larger IKs macroscopic current compared to KCNQ1, recorded in experiments.

To study the effect of KCNE1 on IKs activation during a cardiac ventricular AP, we extracted the fast and slow activation time constants τ_{Pc} (Figure 3.6B) from the structure-based simulations. We incorporated these parameters in a human myocyte model [O'Hara 2011], which was paced at a cycle length of 300ms (Figure 3.4B). In the absence of KCNE1 (Figure 3.4B, left), the KCNQ1 current activates at an early phase of the AP and then declines slowly during the plateau. In contrast, when KCNE1 is present (Figure 3.4B, right), IKs increases monotonically during the plateau to a higher peak amplitude during late plateau and phase-3 repolarization. With this time course, IKs

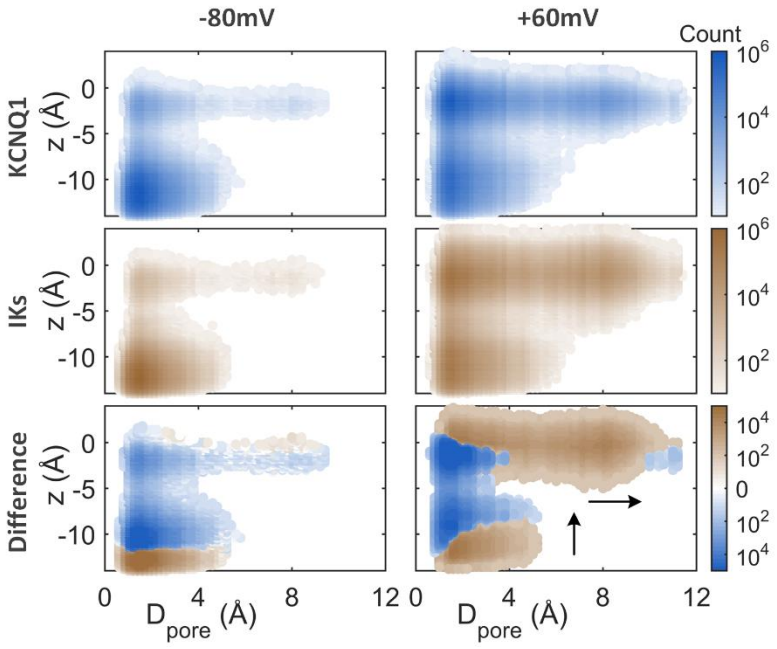

Figure 3.8, Steady-state residency maps of KCNQ1 (top, blue) and IKs (middle, brown) structures projected on the z-D_{pore} plain of configuration space at -80mV (left) and +60mV (right). Maps in the bottom row show the difference between IKs and KCNQ1 residency in the two upper rows. The arrows in the bottom right panel indicate the major directions of conformation changes when the channels are depolarized from -80mV to +60mV. D_{pore}, pore diameter.

provides a large repolarizing current when it is most effective for AP repolarization. The model reproduces the rate adaptation of the AP [O'Hara 2011]; the AP duration (APD) with KCNQ1 is 232ms at cycle length CL = 1000ms and 196ms at CL = 300ms (ΔAPD = 36ms; 15% shortening), with IKs in the absence of β-adrenergic effect APD is 228ms at CL = 1000ms and 182ms at CL = 300ms (ΔAPD = 46ms; 20% shortening) and with β-adrenergic effect APD is 211ms at CL = 1000ms and 165ms at CL = 300ms (ΔAPD = 46ms; 22% shortening). As shown below, IKs is more effective in APD shortening at fast rate than KCNQ1 due to its slower gating properties.

3.4. Contribution of Specific Residues and Structural Elements during Activation Gating

The contribution of each protein residue during activation was evaluated by computing the energy of its electrostatic interactions with the rest of the protein and its self-energy (Figure 3.9). The significant differences of energy contributions by E160 on S2 and by R228 and R237 on S4 in different structures of the VSL library confirm their dominant role in determining conformational changes during activation. KCNE1 does not interact directly with these residues but changes their electrostatic environment (Figure 3.10). This modification results in different rates of transition between VSL conformations in IKs compared to KCNQ1.

Co-assembly of two KCNE1 subunits with KCNQ1 divides the four subunits of KCNQ1 into two different types, based on the proximity of their VSLs to KCNE1 (Figure 2.1C): the VSLs with S3-S4 facing KCNE1 were labeled VS_A and those with S1-S2 facing KCNE1 were labeled VS_B. KCNE1 interacts with charges on VS_A and VS_B with different distances and therefore changes the electrostatic energy landscapes of VS_A and VS_B differently, which results in different average behaviors during membrane depolarization (Figure 3.7). The electrostatic energy contribution of

R249 on S4S5L of VS_A is affected greatly by presence of KCNE1 (see the next section). KCNE1 also influences the electrostatic energy contribution of E146 on S1 of VS_B, and K41 on KCNE1 contributes differently in different VS_B conformations (Figure 3.9, panels B and C). These results indicate an interaction between the N-terminal end of the KCNE1 transmembrane segment and the extracellular portion of S1 in VS_B, as suggested by experiments [Wang 2011, Xu 2013].

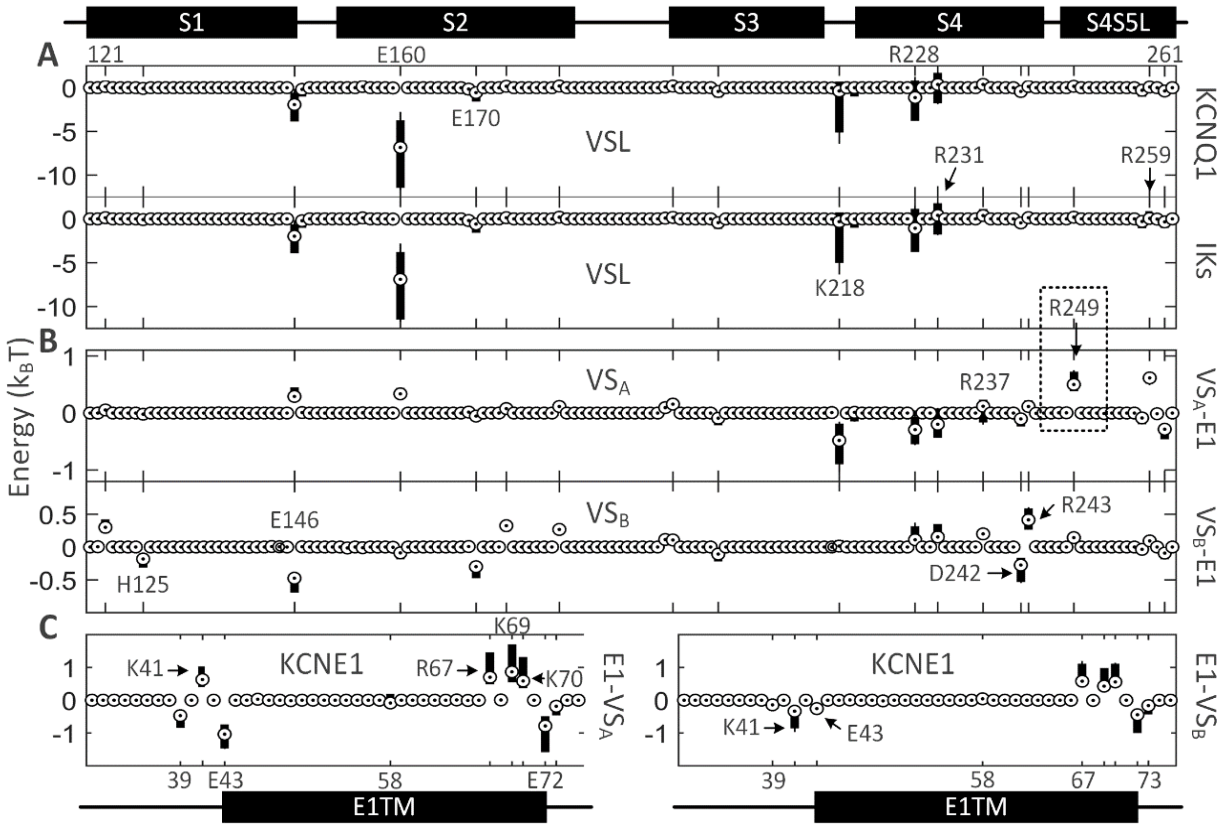

Figure 3.9, Energy contributions from residues on VSL and KCNE1. Energy is computed for interaction between one residue on one subunit and rest of the protein. Median energy is indicated by circle. The bar shows the range of energy over the entire structures in the library. (A) Interactions between residues on VSL and KCNQ1 (top) or IKs (bottom). (B) Interactions between residues on VSL and KCNE1 of IKs (two configurations, VS_A – top and VS_B – bottom). (C) Interactions between residues on KCNE1 and the two types of VS, VS_A – left and VS_B – right. E1TM: KCNE1 transmembrane helix.

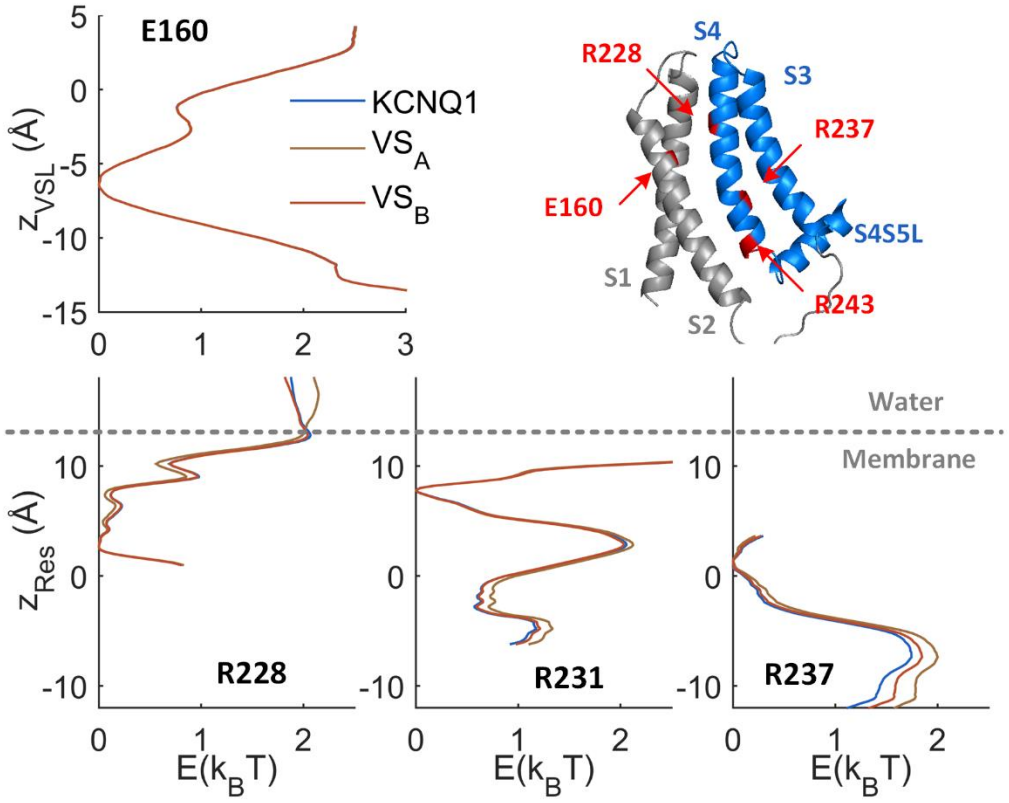

Figure 3.10, Energy contributions as function of z translation, from residues on S2 and S4 without KCNE1 present (KCNQ1 only) and with KCNE1 positioned at different pockets (VS_A and VS_B): E160 on S2 for VSLs at different z levels (z_{VSL}) and R228, R231, R237 on S4 for VSLs at different z levels (z_{Res}).

E160 on S2: The energy minimum locates at a z position where E160 is closest to R231 and the interaction between the negatively charged E160 and all positively charged residues on S4 is maximized. The side chain of E160 could reach a range of z = -2Å to 2Å across the membrane. Note that the three curves are superimposed, which indicates that KCNE1 does not directly interact with E160.

R228 on S4: R228 interacts directly with E160 when VSL is at low z and as it moves into the water-lipid phase. The small local minimum at z_{R228} = 10Å is due to the small distance between R228 and E146 on S1. Presence of additional negative charges from the N-terminal end of KCNE1 transmembrane helix deepens the local minimum in the case of VS_A.

R231 on S4: R231 interacts with E160 at the local minimum z = -1Å. The global minimum for R231 at zR231 = 9Å requires an extreme translocation of VSL across the membrane that has been rarely reached in the simulations.

R237 on S4: R237 gets closer to E160 when VSL moves up; it stabilizes the activated-state VSL conformation at high z.

3.5. Importance of S4S5L in Activation Gating and Coupling between VS and Pore

The calculation of energy contributions from specific residues (Figure 3.9) determines that S4S5L plays an important role in IKs activation (box in Figure 3.9B). When the membrane is depolarized, S4S5L moves with S4 (Figure 3.5); the time constant of its movement coincides with the slow time constant of S4 for both KCNQ1 and IKs (Figure 3.11A). The S4S5L conformational space is limited by its connection to the relatively static S5. A relative movement between S4 and S4S5L is made possible by the dihedral angles of Gly245-Gly246 (Figure 3.11C), which can undergo significant changes due to their small side chains. This enables an initial fast response of S4 to membrane depolarization. It then constraints the additional translation of S4 by coupling it to the swinging movement of S4S5L about the N-terminal end of S5. KCNE1 slows the S4S5L movement and the slow component of S4 movement (z_{S4S5L} and $z_{VS,slow}$ respectively, in Figure 3.11A). The electrostatic interaction between KCNE1 and R249 of S4S5L on VS_A (Figure 3.9B, VS_A-KCNE1) creates an energy barrier at medium S4S5L z displacement and stabilizes it at extreme (low and high) z positions (Figure 3.11B). This impedes the z translation of VS_A and slows IKs activation compared to KCNQ1. During fast pacing of a cardiac myocyte at short CL, the slow S4S5L movement with KCNE1 present could lead to accumulation of channels in conformations with high S4S5L displacements and increased probability for an open pore, creating an “available reserve” of conducting channels. This provides the basis for a larger repolarizing current and shorter APD at fast rate.

S4S5L plays another important role in coupling VS movement and pore opening. The C-terminus of S6 swings beneath S4S5L between its close and open conformations (Figure 3.2). S4S5L contributes to the electrostatic environment of S6; interactions between S4S5L and S6,

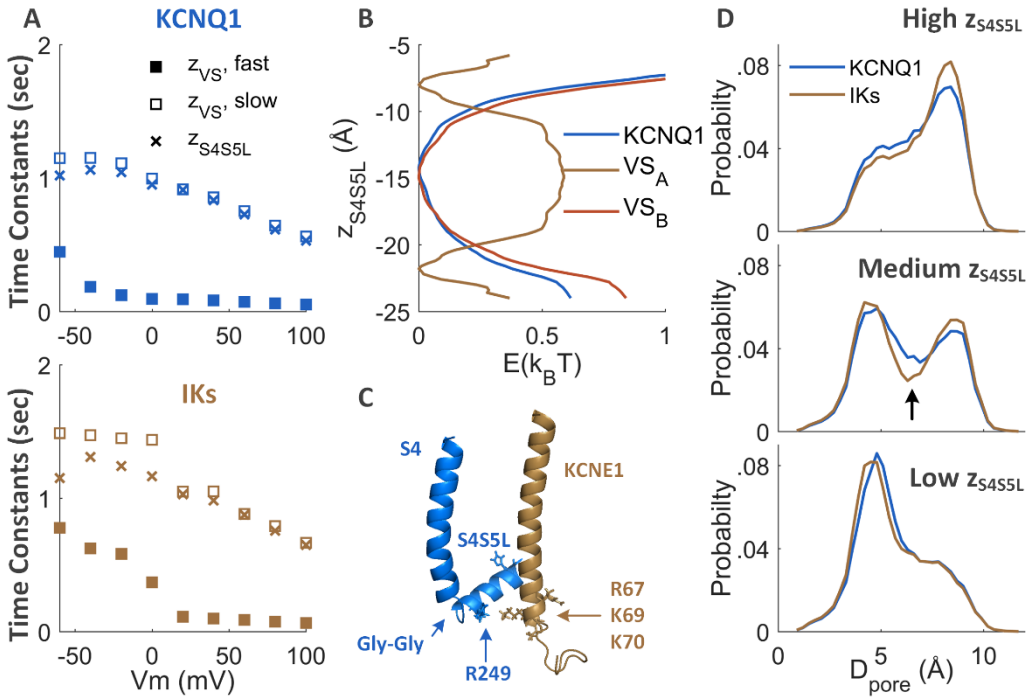

Figure 3.11, (A) Time constants for z translation of VS (z_{VS}, squares) and S4S5L (z_{S4S5L}, x symbols) in KCNQ1 (top) and IKs (bottom) for the protocol in Figure 3.4. There are two time constants for VS movement. The single time constant of S4S5L movement in KCNQ1 and IKs coincides with the slow time constant of VS in both cases. (B) Electrostatic contribution of R249 on S4S5L, with and without KCNE1, at different z levels of S4S5L (z_{S4S5L}). The presence of KCNE1 close to S4S5L of VS_A changes significantly electrostatic energy contribution from R249 and divides the local energy minimum into two minima at extreme positions on the z axis. KCNE1 does not change the electrostatic profile of R249 on S4S5L of VS_B significantly, due to the large distance between these two structural elements. (C) An example VS_A conformation at a medium level of z shows the small distance between R249 and positively charged residues on KCNE1 C-terminus. (D) Average probability of a pore conformation with a particular diameter (D_{pore}) for KCNQ1 (blue) or IKs (brown), with different heights of VSL, z_{S4S5L}. Note that IKs has a smaller probability than KCNQ1 for having medium-size pore conformations (arrow) at medium z_{S4S5L}. This indicates a greater barrier for pore opening as VSL moves up.

both positively charged, favor channel conformations with greater distances between these charges on structural elements. When S4S5L is at medium z, repulsion between these elements impedes pore transitions from close to open conformations (Figure 3.11D, middle). As S4S5L moves up, away from the C-terminal portion of S6, energy preference increases for conformations with a

larger pore (Figure 3.11D, top). The C-terminal end of the KCNE1 transmembrane segment is docked close to S4S5L. It adds positive charge to the space of interaction between S4S5L and S6, decreasing further the probability of transitions from close pore to open pore conformations at medium z positions of S4S5L (Figure 3.11D). Therefore, the presence of KCNE1 requires a higher z position of S4S5L for the channel to be in a conducting state, thereby slowing activation of IKs relative to KCNQ1.

3.6. Discussion

The objectives of this study required an implementation of a computational approach that overcame limitations of existing methods and was capable of simulating ion channel gating over a physiological time scale of its function. This was achieved by dissecting the ion-channel protein into structural segments and linearizing energy computations. We applied this approach to the cardiac IKs channel and studied modulation by the β-subunit KCNE1 of its activation gating. A recent modeling paper introduced a different approach for simulating IKs gating at the atomic scale [Ramasubramanian 2018]. In that approach, artificial intelligence (machine learning) methods were used to overcome the computational enormity of the problem. Reassuringly, the two independent methods generated structural libraries that covered the same conformational space and contained experimentally determined and other simulated structures [Silva 2009, Zaydman 2014, Smith 2007, Wu 2010]. The two approaches were applied to study different aspects of IKs activation.

The simulated trajectories of conformational changes during channel activation reproduced experimental results (Figures 3.4 and 3.6). Further exploration of the conformational library provided new mechanistic insights into the workings of the IKs channel and some of its properties

that have been the subject of a long-standing debate. An important finding confirms that cooperativity between voltage sensors is not required for pore opening in either KCNQ1 or IKs. Not all voltage sensors need to be in activated (up) positions for the channel to be in a conducting state, as the conformational space contains permissible open-pore conformations with one or more voltage sensors in low z positions. However, there is greater preference energetically for open-pore conformations with greater number of activated voltage sensors, increasing their open-pore probability. This property is consistent with the sequential gating concept, proposed in [Meisel 2012]. The KCNE1 transmembrane helix introduces negative charge on the extracellular aspect of the lipid-water phase and positive charge on the intracellular aspect. This modification of the electrostatic environment favors conformations with higher z positions of the positively charged VSLs of IKs, resulting in a larger population of conformations with large pore diameter and larger Pc when KCNE1 is present, resulting in larger macroscopic IKs currents compared to KCNQ1 [Sanguinetti 1996]. To study this property experimentally, it will be useful to devise fluorescent signal recording experiments that can identify channel conformations with different numbers of H-VSLs and record their occurrence together with macroscopic KCNQ1 and IKs currents.

Like other voltage-gated potassium channels [Papazian 1995], the positively charged S4 segment of KCNQ1 moves up across the membrane in response to depolarization. Experimental studies suggested an important role for S4S5L in IKs gating [Choveau 2011, Labro 2011, Lvov 2010, Sun 2017]. This functional property of S4S5L is supported by the residue-specific energy analysis of electrostatic interactions (Figure 3.9). The correspondence of the slow component of VSL movement with the upward movement of S4S5L (Figure 3.11) implies restriction of late-phase S4 movement by S4S5L due to the short linker between them. The slowing of S4S5L movement and thereby of the slow component of S4 by KCNE1, provides an explanation for the

detection of 2-stage VS movement in fluorescence experiments for IKs but not for KCNQ1 [Barro-Soria 2014]. The fast stage of the VS movement that is not slowed by the S4S5L movement, covers a larger displacement compared to the slow stage. This result is consistent with the observation by [Ramasubramanian 2018]. Direct experimental evaluation of the role of S4S5L movement during activation gating is difficult to obtain because of its cytosolic position on the channel protein.

Previous experiments concluded that KCNE1 slows KCNQ1 activation either by slowing the S4 movement [Ruscic 2013] or by suppressing the coupling between VS movement and pore opening [Osteen 2010, Barro-Soria 2014]. The simulations demonstrated coexistence of both mechanisms and determined their molecular basis (Figure 3.6 and 3.11). Slowing of IKs S4S5L movement, by the interaction between its R249 residue and the C-terminus of the KCNE1 transmembrane segment, has two consequences – it slows S4 movement and delays pore opening. Compared to KCNQ1, IKs requires a larger S4S5L movement to a higher position to achieve Pc larger than 0.5. Coupling between VS movement and pore opening is reduced, delaying IKs activation. A previous experiment suggested the presence of an intermediate-open state in KCNQ1 but not in IKs [Zaydman 2014]. The simulated trajectories in the present study support this observation, identifying many more conducting conformations with VSLs at middle-z positions in KCNQ1 than in IKs. While open conformations with VS in middle z are possible, they occur with small probability because of the barrier to transition from close to open pore (Figure 3.11D, middle).

The ratio of KCNQ1:KCNE1 was assumed 4:2, considered the dominant stoichiometry of IKs in cardiac cells [Plant 2014]. With two KCNE1 subunits located in opposite pockets of the KCNQ1 tetramer, the four VSLs that are symmetric in KCNQ1, can be divided into two types, VS_A and VS_B. The simulations show that KCNE1 modifies the electrostatic energy landscapes of these two

VSLs in two different ways (Figure 3.7). Electrostatic interaction with the C-terminus of KCNE1 transmembrane helix favors extreme z positions for S4S5L in VS_A, but does not affect the S4S5L in VS_B significantly. Consequently, the two types of VSLs in IKs behave differently during channel activation, a behavior that was also observed in recent simulations using a different, independent approach [Ramasubramanian 2018]. This property could contribute to the multiple stages of IKs voltage dependent gating observed experimentally [Barro-Soria 2014]. The possibility of variable KCNQ1:KCNE1 has also been suggested [Nakajo 2010, Murray 2016]. On-going simulations, using the computational approach presented here, could examine the hypothesis that variable stoichiometry is a mechanism for modulation of IKs function.

3.7. Limitations

The emphasis in this study was on the transmembrane domain of the KCNQ1/KCNE1 complex. Only spatial occupation by the cytosolic domain was considered in the study, including Helix-A, Helix-B, Helix-C, Calmodulin, KCNE1 C-terminus and a docked PIP2. The electrostatic energy from the cytosolic domain of KCNQ1 was neglected, considering the screening effect of the water phase. In order to linearize the electrostatic energy calculation for the transmembrane domain, parameters were estimated from a coarse-grid sample set of the conformation library. We estimated the error introduced by the linearization to be smaller than 1.5%. We evaluated the channel conductance indirectly, based on the pore diameter as a surrogate. Single-channel recordings detected multiple subconductances of IKs [Werry 2013]; subconductances will be introduced in the simulations from structural considerations when more detailed information on the pore structure becomes available. The simulations were conducted with a fixed 4:2 KCNQ1:KCNE1 stoichiometry, considered the dominant ratio under physiological conditions.

Studying other stoichiometries (we hypothesize that stoichiometry could be variable and serves to regulate channel function [Nakajo 2010, Murray 2016]) requires building structural libraries for each stoichiometry from 4:1 to 4:4. A study of variable stoichiometry, considering all possible configurations of KCNE1 docking in KCNQ1, is being conducted in our laboratory.

Chapter 4 Concluding Remarks and Suggestions for Future Studies

This is the first study that integrates the dynamics of an ion-channel protein structure into a model of the whole-cell AP. A previous modeling study used a Markov model of IKs kinetics to examine its role in AP repolarization [Silva 2005]. Here, starting from the molecular protein structure and its conformational changes during activation, we compare the time course of IKs and KCNQ1 during a human ventricular AP (Figure 3.4B). The results demonstrate that modulation by KCNE1 is essential for an effective role of IKs in AP repolarization and AP shortening at fast rate.

The computational framework presented here is general and could be applied to study the relationships between physiological function and molecular structure of a variety of proteins. Examples specific to IKs could include: (1) The structural libraries of KCNQ1 and IKs generated here could be used to study other properties of the wild-type ion channel (e.g., the possible regulatory role of KCNQ1:KCNE1 stoichiometry; dependence on potassium ion concentration). (2) Following the same scheme, structural libraries could be generated for channels containing mutations to study the structural basis of pathological phenotypes such as the long QT syndrome. (3) Similarly, libraries of structures modified by drug binding could be used to study drug action and drug toxicity. (4) Effects of other regulatory subunits (e.g. KCNE2) could be explored. (5) The mechanism of β-adrenergic stimulation and current amplification could be studied, once methods are developed to extend the approach to the unstructured N-terminus of KCNQ1.

4.1. Stoichiometry

The stoichiometry of the I_{Ks} channel is still being debated. Morin and Kobertz [Morin 2008] show that a functional KCNQ1/KCNE1 channel has two KCNE1 accessory units co-assembled with the four pore-forming KCNQ1 subunits. An elevated KCNE1 concentration found in patients with chronic heart failure exhibits slowed activation kinetics and a positive shift in the voltage dependence of the macroscopic current compared to the normal case, suggesting a changed stoichiometry of the KCNQ1/KCNE complex [Watanabe 2007]. A recent fluorescent study shows a flexible ratio of KCNQ1 to KCNE1 in the channel and its dependence on the relative expression levels of the two components, which may play a role in regulating the heart rhythm [Nakajo 2010, Nakajo 2011]. Furthermore, expression experiment over a long time of KCNQ1 with KCNE1 shows gradual changes in the macroscopic current characteristics at different time points, indicating a gradual disappearance of KCNE1 subunits from the cell membrane and a reversible behavior of KCNQ1-KCNE1 co-assembly [Poulsen 2007]. In contrast to the hypothesis in the simulations above that the stoichiometry is fixed at 4:2 under physiological conditions, another hypothesis of variable stoichiometry could be examined by the following protocols:

(1) Repeat the procedures in Chapter 2 to construct structural libraries of 6 different configurations of KCNQ1/KCNE1 complex (including KCNQ1 only, Figure 4.1) of which two libraries have been completed in this study (KCNQ1 and IKs_O in Figure 4.1).

(2) Trajectories of conformational changes during gating of different configurations with different stoichiometries could be computed using the different libraries. Voltage dependence and time constants of the VS movement and the probability of a conducting pore conducting for KCNQ1, IKs1, IKsO and IKs4 could be validated by comparison to a recent fluorescent study [Murray 2016].

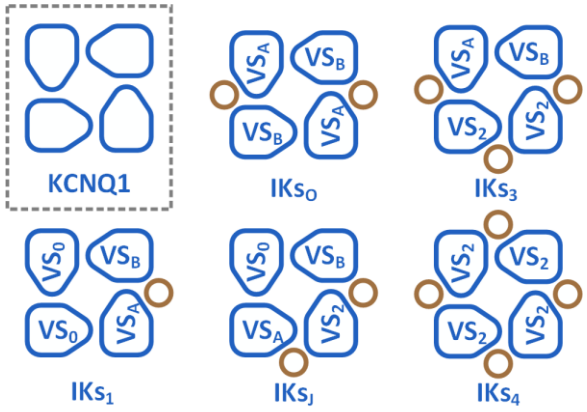

Figure 4.1, Configurations of KCNQ1/KCNE1 complex with different stoichiometries. VS_0, VS_A, VS_B and VS_2 denote different types of the VS of KCNQ1, differentiated according to their location relative to KCNE1 in the protein. IKs_O is the IKs in the previous chapters.

(3) x_{s1} and x_{s2} in equation (2.9) could be re-computed based on the generated trajectories to formulate the equation calculating each component in the equation below:

$$IKs = k_{Q1}[KCNQ1] + k_1[IKs_1] + k_O[IKs_O] + k_J[IKs_J] + k_3[IKs_3] + k_4[IKs_4] \qquad (4.1)$$

where k_x is the percentage of each component and [KCNQ1] or [IKs_x] are the currents carried by the different components, computed by equation (2.9) with different x_{s1} and x_{s2} for each configuration. If we express the same amount of KCNQ1 and KCNE1 in the cell and assume that there is no cooperativity in co-assembly of KCNQ1 and KCNE1, we have $k_{Q1} = 0.053$, $k_1 = 0.249$, $k_O = 0.132$, $k_J = 0.263$, $k_3 = 0.249$ and $k_4 = 0.053$. When the expression level of KCNE1 increases, larger k_O, k_J, k_3 and k_4 are expected and the cell is anticipated to have a slower activating I_{Ks} current and a longer AP duration [Watanabe 2007].

4.2. Mutation Studies

Simulations of I_{Ks} channels carrying mutations could help to validate the molecular and cellular models and to examine the hypotheses presented here. KCNQ1 I257 on the S4-S5 linker, H363 on S6, and H73, S74, D76 on KCNE1 are important residues in the interaction between the gating structure of KCNQ1 and the C-terminal part of the KCNE1 transmembrane helix. It is expected

that mutations on these sites would affect the channel activation. The mutation G52R, located above the middle point of the KCNE1 transmembrane segment, is associated with LQT5. The mutated KCNE1 co-assembles with the KCNQ1 subunits, but generates a macroscopic current with kinetics similar to the KCNQ1 channel [Harmer 2010].

The first step in mutation studies is to construct a structural model of the KCNQ1/KCNE1 complex carrying a specific point mutation, for example, with Gly52 on KCNE1 substituted by an Arginine residue. With the mutation, the docking site of KCNE1 in KCNQ1 may require a fine adjustment, which could be calculated through the docking procedures described above. By using the methods described above, energy landscape with S4 at different positions in the structure of mutated IKs at different membrane potentials will be calculated to obtain activation gates in the macroscopic current model corresponding to the mutation. Comparing the current traces generated by the modified "mutant" model and experimental data, the level of consistency will provide a measure of accuracy for the following hypotheses regarding phenotypes of LQT mutations: (1) Insertion of a positive charge in the middle part of the KCNE1 transmembrane segment (G52R) will interfere with the interaction between the hydrophobic side chains of KCNQ1 and KCNE1 and increase the distance between the C-terminus of the KCNE1 transmembrane helix and the S4-S5 linker of KCNQ1. This will remove the obstacle that slows the S4-S5 linker movement during gating and the mutant channel will generate a macroscopic current with fast activation, similar to the KCNQ1 channel [Harmer 2010]; (2) Mutation S74L on KCNE1 shares similarities in the side chains with Ile257 on the S4-S5 linker of KCNQ1, with which Ser74 on KCNE1is shown to make contact. This suggests KCNE1's role in impeding the movement of the S4-S5 linker by increasing the size of the KCNE1 side chains. It slows activation of the mutated channel and produces a

positive shift in the voltage dependence of the IKs current, prolonging the APD and the QT interval on the patient's ECG [Chen 2009].

4.3. Potential Requirements for Computational Resources

Our computational framework could be extended into areas studying the relationships between physiological function and molecular structure of proteins other than IKs. The two key procedures of the presented approach are construction of a structural library and generation of trajectories for conformational changes under various voltage protocols. The time to execute the first step is highly dependent on the number of degrees of freedom of the target protein, the desired resolution of the library and knowledge of the conformational space. The second step is less time consuming and depends on the number of trajectories required for convergence. Taking the IKs conformation library in this study as an example, it requires about 8 weeks for a 64-core super-computer to construct the raw library. Applying restrictions to the library (eliminating steric clashes, etc.) takes additional time. It requires another 2-3 weeks of computing time to generate the trajectories. Building a Hodgkin-Huxley model of the current and incorporation into the cell model requires minimal computational resources and could be accomplished using a desktop computer within one week. Note that it is possible to optimize these procedures by specialized data structures and computational algorithms.

References

- Ansari A. Mean first passage time solution of the Smoluchowski equation: Application to relaxation dynamics in myoglobin. The Journal of Chemical Physics 2000; 112(5): 2516-2522.
- Barhanin J, Lesage F, Guillemare E, Fink M, Lazdunski M, Romey G.K(V)LQT1 and lsK (minK) proteins associate to form the I(Ks) cardiac potassium current. Nature. 1996 Nov 7;384(6604):78-80.
- Barro-Soria R, Rebolledo S, Liin SI, Perez ME, Sampson KJ, Kass RS, et al. KCNE1 divides the voltage sensor movement in KCNQ1/KCNE1 channels into two steps. Nat Commun 2014; 5: 3750.
- Bartos DC, Morotti S, Ginsburg KS, Grandi E, Bers DM. Quantitative analysis of the Ca2+ -dependent regulation of delayed rectifier K+ current IKs in rabbit ventricular myocytes. J Physiol 2017; 595(7):2253-2268.
- Chen J, Zheng R, Melman YF, McDonald TV. Functional interactions between KCNE1 C-terminus and the KCNQ1 channel. PLoS One. 2009;4(4):e5143.
- Choveau FS, Rodriguez N, Ali FA, Labro AJ, Rose T, Dahimène S, et al. KCNQ1 channels voltage dependence through a voltage-dependent binding of the S4-S5 linker to the pore domain. J Biol Chem 2011; 286(1): 707-716.
- Chung DY, Chan PJ, Bankston JR, Yang L, Liu G, Marx SO, et al. Location of KCNE1 relative to KCNQ1 in the I(KS) potassium channel by disulfide cross-linking of substituted cysteines. Proc Natl Acad Sci USA 2009; 106(3): 743-748.
- Dolinsky TJ, Nielsen JE, McCammon JA, Baker NA. PDB2PQR: an automated pipeline for the setup, execution, and analysis of Poisson-Boltzmann electrostatics calculations. Nucleic Acids Research 2004; 32: W665-W667.
- Harmer SC, Wilson AJ, Aldridge R, Tinker A. Mechanisms of disease pathogenesis in long QT syndrome type 5. Am J Physiol Cell Physiol. 2010 Feb;298(2):C263-73.
- Heijman J, Volders PG, Westra RL, Rudy Y. Local control of β-adrenergic stimulation: Effects on ventricular myocyte electrophysiology and Ca(2+)-transient. J Mol Cell Cardiol. 2011; 50(5): 863-71.
- Im W, Feig M, Brooks CL 3rd. An implicit membrane generalized born theory for the study of structure, stability, and interactions of membrane proteins. Biophys J 2003; 85(5): 2900-2918.
- Jensen MØ, Jogini V, Borhani DW, Leffler AE, Dror RO, Shaw DE. Mechanism of voltage gating in potassium channels. Science 2012; 336(6078): 229-233.

- Jespersen T, Grunnet M, Olesen SP. The KCNQ1 potassium channel: from gene to physiological function. Physiology (Bethesda). 2005 Dec;20:408-16.
- Kang C, Tian C, Sönnichsen FD, Smith JA, Meiler J, George AL Jr, et al. Structure of KCNE1 and implications for how it modulates the KCNQ1 potassium channel. Biochemistry 2008; 47(31): 7999-8006.
- Labro AJ, Boulet IR, Choveau FS, Mayeur E, Bruyns T, Loussouarn G, et al. The S4-S5 linker of KCNQ1 channels forms a structural scaffold with the S6 segment controlling gate closure. J Biol Chem 2011; 286(1): 717-725.
- Larkin MA, Blackshields G, Brown NP, Chenna R, McGettigan PA, McWilliam H, et al. Clustal W and Clustal X version 2.0. Bioinformatics 2007; 23(21): 2947-2948.
- Long SB, Tao X, Campbell EB, MacKinnon R. Atomic structure of a voltage-dependent K+ channel in a lipid membrane-like environment. Nature 2007; 450(7168): 376-382.
- Luo CH, Rudy Y. A dynamic model of the cardiac ventricular action potential. I. Simulations of ionic currents and concentration changes. Circ Res. 1994 Jun;74(6):1071-96.
- Lvov A, Gage SD, Berrios VM, Kobertz WR. Identification of a protein-protein interaction between KCNE1 and the activation gate machinery of KCNQ1. J Gen Physiol 2010; 135(6): 607-618.
- Martí-Renom MA, Stuart AC, Fiser A, Sánchez R, Melo F, Sali A. Comparative protein structure modeling of genes and genomes. Annu Rev Biophys Biomol Struct 2000; 29: 291-325.
- Meisel E, Dvir M, Haitin Y, Giladi M, Peretz A, Attali B. KCNQ1 channels do not undergo concerted but sequential gating transitions in both the absence and the presence of KCNE1 protein. J Biol Chem 2012; 287(41): 34212-24.
- Mikuni I, Torres CG, Bienengraeber MW, Kwok WM. Partial restoration of the long QT syndrome associated KCNQ1 A341V mutant by the KCNE1 β-subunit. Biochim Biophys Acta 2011; 1810(12): 1285-1293.
- Morin TJ, Kobertz WR. Counting membrane-embedded KCNE beta-subunits in functioning K+ channel complexes. Proc Natl Acad Sci U S A. 2008 Feb 5;105(5):1478-82.
- Murray CI, Westhoff M, Eldstrom J, Thompson E, Emes R, Fedida D. Unnatural amino acid photo-crosslinking of the IKs channel complex demonstrates a KCNE1:KCNQ1 stoichiometry of up to 4:4. Elife. 2016 Jan 23;5. pii: e11815.
- Nakajo K, Kubo Y. Nano-environmental changes by KCNE proteins modify KCNQ channel function. Channels (Austin). 2011 Sep 1;5(5).
- Nakajo K, Kubo Y. Steric hindrance between S4 and S5 of the KCNQ1/KCNE1 channel hampers pore opening. Nat Commun 2014; 5: 4100.

- Nakajo K, Ulbrich MH, Kubo Y, Isacoff EY. Stoichiometry of the KCNQ1 - KCNE1 ion channel complex. Proc Natl Acad Sci U S A. 2010 Nov 2;107(44):18862-7.
- Nekouzadeh A, Rudy Y. Continuum molecular simulation of large conformational changes during ion-channel gating. PLoS One 2011; 6(5): e20186.
- Nekouzadeh A, Rudy Y. Conformational changes of an ion-channel during gating and emerging electrophysiologic properties: Application of a computational approach to cardiac Kv7.1. Prog Biophys Mol Biol 2016; 120(1-3): 18-27.
- Nekouzadeh A, Silva JR, Rudy Y. Modeling subunit cooperativity in opening of tetrameric ion channels. Biophys J 2008; 95 (7): 3510-20.
- O'Hara T, Virág L, Varró A, Rudy Y. Simulation of the undiseased human cardiac ventricular action potential: model formulation and experimental validation. PLoS Comput Biol 2011; 7(5): e1002061.
- Osteen JD, Gonzalez C, Sampson KJ, Iyer V, Rebolledo S, Larsson HP, et al. KCNE1 alters the voltage sensor movements necessary to open the KCNQ1 channel gate. Proc Natl Acad Sci USA 2010; 107(52): 22710-22715.
- Panaghie G, Purtell K, Tai KK, Abbott GW. Voltage-dependent C-type inactivation in a constitutively open K+ channel. Biophys J 2008; 95(6): 2759-2778.
- Papazian DM, Shao XM, Seoh SA, Mock AF, Huang Y, Wainstock DH. Electrostatic interactions of S4 voltage sensor in Shaker K+ channel. Neuron 1995; 14(6): 1293-1301.
- Phillips JC, Braun R, Wang W, Gumbart J, Tajkhorshid E, Villa E, et al. Scalable molecular dynamics with NAMD. J Comput Chem 2005; 26(16): 1781-1802.
- Plant LD, Xiong D, Dai H, Goldstein SA. Individual IKs channels at the surface of mammalian cells contain two KCNE1 accessory subunits. Proc Natl Acad Sci USA 2014; 111(14): E1438-1446.
- Poulsen AN, Klaerke DA. The KCNE1 beta-subunit exerts a transient effect on the KCNQ1 K+ channel. Biochem Biophys Res Commun. 2007 Nov 9;363(1):133-9.
- The PyMOL Molecular Graphics System, Version 1.3 Schrödinger, LLC.
- Ramasubramanian S, Rudy Y. The Structural Basis of IKs Ion-Channel Activation: Mechanistic Insights from Molecular Simulations. Biophys J 2018; 114(11): 2584-2594
- Rudy Y, Silva JR. Computational biology in the study of cardiac ion channels and cell electrophysiology. Q Rev Biophys 2006; 39(1): 57-116.
- Ruscic KJ, Miceli F, Villalba-Galea CA, Dai H, Mishina Y, Bezanilla F, et al. IKs channels open slowly because KCNE1 accessory subunits slow the movement of S4 voltage sensors in KCNQ1 pore-forming subunits. Proc Natl Acad Sci USA 2013; 110(7): E559-566.

- Sachyani D, Dvir M, Strulovich R, Tria G, Tobelaim W, Peretz A, et al. Structural basis of a Kv7.1 potassium channel gating module: studies of the intracellular c-terminal domain in complex with calmodulin. Structure 2014; 22(11): 1582-1594.
- Sahu ID, Craig AF, Dunagan MM, Troxel KR, Zhang R, Meiberg AG, et al. Probing Structural Dynamics and Topology of the KCNE1 Membrane Protein in Lipid Bilayers via Site-Directed Spin Labeling and Electron Paramagnetic Resonance Spectroscopy. Biochemistry 2015; 54(41): 6402-6412.
- Sahu ID, Kroncke BM, Zhang R, Dunagan MM, Smith HJ, Craig A, et al. Structural investigation of the transmembrane domain of KCNE1 in proteoliposomes. Biochemistry 2014; 53(40): 6392-6401.
- Sanguinetti MC, Curran ME, Zou A, Shen J, Spector PS, Atkinson DL, et al. Coassembly of K(V)LQT1 and minK (IsK) proteins to form cardiac I(Ks) potassium channel. Nature 1996; 384(6604): 80-83.
- Silva JR, Pan H, Wu D, Nekouzadeh A, Decker KF, Cui J, et al. A multiscale model linking ion-channel molecular dynamics and electrostatics to the cardiac action potential. Proc Natl Acad Sci USA 2009; 106(27): 11102-11106.
- Silva J, Rudy Y. Subunit interaction determines IKs participation in cardiac repolarization and repolarization reserve. Circulation 2005; 112(10): 1384-91.
- Smith JA, Vanoye CG, George AL Jr, Meiler J, Sanders CR. Structural models for the KCNQ1 voltage-gated potassium channel. Biochemistry 2007; 46(49): 14141-14152.
- Still WC, Tempczyk A, Hawley RC, Hendrickson T. Semianalytical treatment of solvation for molecular mechanics and dynamics. J Am Chem Soc 1990; 112(16): 6127-6129.
- Strutz-Seebohm N, Pusch M, Wolf S, Stoll R, Tapken D, Gerwert K, et al. Structural basis of slow activation gating in the cardiac I Ks channel complex. Cell Physiol Biochem 2011; 27(5): 443-452.
- Sun J, MacKinnon R. Cryo-EM Structure of a KCNQ1/CaM Complex Reveals Insights into Congenital Long QT Syndrome. Cell 2017; 169(6): 1042-1050.
- Tapper AR, George AL Jr. Location and orientation of minK within the I(Ks) potassium channel complex. J Biol Chem 2001; 276(41): 38249-38254.
- Terrenoire C, Clancy CE, Cormier JW, Sampson KJ, Kass RS. Autonomic control of cardiac action potentials: role of potassium channel kinetics in response to sympathetic stimulation. Circ Res. 2005 Mar 18;96(5):e25-34.
- Tombola F, Pathak MM, Isacoff EY. How far will you go to sense voltage? Neuron 2005; 48(5): 719-725.
- Wang Q, Curran ME, Splawski I, Burn TC, Millholland JM, VanRaay TJ, Shen J, Timothy KW, Vincent GM, de Jager T, Schwartz PJ, Toubin JA, Moss AJ, Atkinson DL, Landes GM,

Connors TD, Keating MT. Positional cloning of a novel potassium channel gene: KVLQT1 mutations cause cardiac arrhythmias. Nat Genet. 1996 Jan;12(1):17-23.

- Wang YH, Jiang M, Xu XL, Hsu KL, Zhang M, Tseng GN. Gating-related molecular motions in the extracellular domain of the IKs channel: implications for IKs channelopathy. J Membr Biol 2011; 239(3): 137-156.
- Watanabe E, Yasui K, Kamiya K, Yamaguchi T, Sakuma I, Honjo H, Ozaki Y, Morimoto S, Hishida H, Kodama I. Upregulation of KCNE1 induces QT interval prolongation in patients with chronic heart failure. Circ J. 2007 Apr;71(4):4s71-8.
- Werry D, Eldstrom J, Wang Z, Fedida D. Single-channel basis for the slow activation of the repolarizing cardiac potassium current, I(Ks). Proc Natl Acad Sci USA 2013; 110(11): E996-1005.
- Wu D, Delaloye K, Zaydman MA, Nekouzadeh A, Rudy Y, Cui J. State-dependent electrostatic interactions of S4 arginines with E1 in S2 during Kv7.1 activation. J Gen Physiol 2010; 135(6): 595-606.
- Xu Y, Wang Y, Meng XY, Zhang M, Jiang M, Cui M, et al. Building KCNQ1/KCNE1 channel models and probing their interactions by molecular-dynamics simulations. Biophys J 2013; 105(11): 2461-2473.
- Yang WP, Levesque PC, Little WA, Conder ML, Shalaby FY, Blanar MA. KvLQT1, a voltage-gated potassium channel responsible for human cardiac arrhythmias. Proc Natl Acad Sci U S A. 1997 Apr 15;94(8):4017-21.
- Zaydman MA, Kasimova MA, McFarland K, Beller Z, Hou P, Kinser HE, et al. Domain-domain interactions determine the gating, permeation, pharmacology, and subunit modulation of the IKs ion channel. Elife 2014; 3: e03606.

Appendix

A1. List of Abbreviations

- AP, action potential.
- APD, action potential duration.
- CaM, calmodulin.
- D_{pore}, pore diameter of a KCNQ1 conformation.
- ECG, electrocardiogram.
- HR, His258-Arg259 of KCNQ1.
- H-VSL, voltage sensor and S4-S5 Linker (VSL) locates at high z positions.
- ISO, isoproterenol.
- LQT syndrome (or Long QT syndrome), syndrome with a prolonged QT interval in a patient's ECG signal.
- LQT1, LQT syndrome type1.
- L-VSL, voltage sensor and S4-S5 Linker (VSL) locates at low z positions.
- MD, molecular dynamics.
- NMR, nuclear magnetic resonance spectroscopy.
- PAG, Pro343-Ala344-Gly345 of KCNQ1.
- Pc, probability for a conformation to be in a conducting state.
- QGG, Gln244-Gly245-Gly246 of KCNQ1.
- RMSD, root-mean-square deviation
- S4S5L, S4-S5 linker.

- S6N, N-terminal section of S6, residues 323-342 of KCNQ1
- S6C, C-terminal section of KCNQ1 S6 after PAG.
- Vm, membrane voltages.
- VS, voltage sensor, S3-S4 domain in KCNQ1.
- VSL, voltage sensor and S4-S5 Linker.
- VS_X, different types of the VS of KCNQ1, differentiated according to their location relative to KCNE1 in the protein

A2. Additional Information of Parameters and Variables

- Van der Waals radii of atoms: C, 1.70Å; O, 1.52Å; N, 1.55Å; H, 1.20Å; S, 1.80Å.
- Boundaries of membrane-water boxes for MD simulations: x, [-70Å 70Å]; y, [-70Å 70Å]; z, [-90Å 50Å] (more space in the cytosolic side of the protein).
- Temperatures: 0K for initialization of MD simulations and 310K for all the other cases.
- Force field: CHARMM2.7 (https://www.charmm.org/charmm/).
- Computing electrostatic energy: (1) Distribution of partial charges on a certain atom in a residue and occupation of that atom carrying such partial charges was generated by PDB2PQR Server (http://nbcr-222.ucsd.edu/pdb2pqr_2.0.0/) [Dolinsky 2004]. (2) Coulomb's constant $k_e = 8.99\times10^9$ $N\cdot m^2/C^2$ = 332.057 kcal· Å/mol. (3) Dielectric constant of protein and membrane $\varepsilon_p = 2.0$, dielectric constant of water $\varepsilon_w = 80.0$.

A3. Data Profile

Due to the large data size, it is impossible to attach the source files directly to the dissertation. However, we will publish the core dataset with the source code on our website (rudylab.wustl.edu)

to help others to reconstruct the entire conformational library used in this work. Instructions how to generate the trajectories or modify the library will also be made available with the code.